

Simple Book Example

TeXstudio Team

January 2013

ii

thesis

Contents

1	Simulation of a plenoptic 2.0 system	1
1.1	Rendering in Plenoptic 2.0	2
1.1.1	Extracting sub images	4
1.1.2	Basic Rendering	5
1.1.3	Depth based rendering	7
1.2	Description of the system	10
1.3	Optical performances of a focused plenoptic system	15
1.4	Impulse response of a Focused Plenoptic system	19
1.5	Two point resolution	23
1.6	Frequency analysis of a focused plenoptic system	27
1.7	Conclusions	42

List of Figures

1.1	Top: the point A is imaged by the main lens into the point A' . A' is imaged by the lens let array into a number of sub images depending by the magnification of the micro array stage, in this case $m=0.333$. Bottom: particular of the raw image at the point source A and phase space diagram. The three sub images 1,2 and 3 are three different points of view of the object.	3
1.2	Relation between the position of the centre of a lens let x and the position of the centre of the correspondent sub image $x + x'$	5
1.3	Basic rendering algorithm. The Rendered image is composed tiling together patches extracted by each sub image. The patch size is dependent by the magnification of the micro array stage.	6
1.4	The points that belongs to the object plane represented in red are imaged on a virtual main lens image plane. This plane is relayed on a virtual sensor plane by a virtual micro array whose parameters are a' and b' and $m' = b'/a'$	8
1.5	9
1.6	Ray diagram of the system simulated.	10
1.7	Values of the parameter b correspondent to values of magnification varying from 0.1 to 0.5.	12
1.8	Values of the parameter b corresponding to values of magnification varying from 0.1 to 0.5.	13
1.9	Aperture of the main lens as a function of the magnification in order to respect the f-number matching condition.	14
1.10	Aperture of the main lens as a function of the magnification in order to respect the f-number matching condition.	16
1.11	lateral resolution as a function of the magnification.	18
1.12	optical cut-off frequency as a function of the magnification.	18

1.13 Left: raw sensor image, Right: rendered image. Artifacts are present. Magnification: 0.5	20
1.14 Left: raw sensor image, Right: rendered image. Artifacts are present. Magnification: 0.3.	20
1.15 Left: raw sensor image, Right: rendered image. Artefacts are present. Magnification: 0.25	21
1.16 From top to bottom: comparison between the main lens image profile, in blue, and the rendered image profile, in red, for magnification values of 0.5,0.3 and 0.25. The central lobe of the rendered image increase with the magnification, as well as the number of artefacts.	22
1.17 On the top left there is the main lens image of two point sources separated by the Rayleigh distance δx . On the top right its corresponded rendered plenoptic image obtained with a magnification of 0.5. As expected from the theory, the resolution of the rendered image is half the one af the main lens image, and the two points are no more distinguishable as confirmed by the intensity profiles of the two images on the bottom.	25
1.18 The image on the top left shows the main lens image of two point sources separated by the Rayleigh distance $2\delta x$. On the top right there is its corresponded rendered plenoptic image obtained with a magnification of 0.5. Doubling the Rayleigh distance the rendered image is at the limit of resolution, where the maximum of the Airy pattern of one point falls on the first zero of the second point.	26
1.19 Modulation transfer functions of the main lens (green) and the overall imaging system (red) for a magnification value of $m = 0.5$, top, $m = 0.3$, central, and $m = 0.25$, bottom.	29
1.20 The object imaged in this simulation is a sinusoidal grating containing five different frequencies.	31
1.21 Top: on the left it is shown the raw sensor image, on the right the main lens image. Bottom: On the left there is the rendered image, on the right the same image has been low pass filtered to remove some of the rendering artefacts. Magnification was 0.5	32

1.22 On the left: intensity profiles of the main lens image, top and of the rendered image, bottom. On the right the spatial frequencies modulated according to the MTF as shown by the power spectra of the main lens image on the top right and of the rendered image on the bottom right. The magnification of the lens let array is $m = 0,5$ and cut-off frequency of the system is $f_{cut-off} = 10^4 m - 1$	33
1.23 Evolution of the spectrum of the optical field as it propagates through the imaging system. First step the field is propagated through the main lens and its frequency content is modulated by its MTF whose bandwidth is $\Delta\nu_1$. Then modulated field passes through the lens let array stage and because of the magnification that is less than zero its bandwidth is reduced further to $\Delta\nu_2$. Since $\nu_1 < \nu_2$ the imaging system is modelled as a linear low pass filter with a bandwidth $\Delta\nu_1$ defined by the magnification of the micro array stage.	35
1.24 Top: on the left it is shown the raw sensor image, on the right the main lens image. Bottom: On the left there is the rendered image, on the right the same image has been low pass filtered to remove some of the rendering artefacts. Magnification was 0.3.	37
1.25 On the left: intensity profiles of the main lens image, top and of the rendered image, bottom. On the right: spatial frequency modulation done by MTF. The cut-off frequency of the system is $0.756 \times 10^4 m - 1$	38
1.26 Aliased frequencies transmitted to the rendered image.	39
1.27 Top: raw sensor image, on the right the main lens image. Bottom: On the left there is the rendered image, on the right the same image has been low pass filtered to remove some of the rendering artefacts. Magnification was 0.3.	40
1.28 On the left: intensity profiles of the main lens image, top and of the rendered image, bottom. On the right there are the spatial frequencies modulated according to the MTF. The cut-off frequency of the system is $0.6 \times 10^4 1/m$	41

Chapter 1

Simulation of a plenoptic 2.0 system

In this chapter several simulations performed to characterize the optical performances of a focused plenoptic imaging system will be presented. The scope of this work is to investigate the behaviour of a plenoptic 2.0 imaging system at its diffraction limit under a wave optics approach. All simulations described in this chapter have been run using the Fresnel Simulation Toolbox described in chapter ???. In a plenoptic 1.0 imaging system the resolution is limited by the dimensions of the lens lets [37] and the final rendered image has a much lower resolution than a conventional image. In a focused plenoptic system, as explained in section ???, the resolution of the final rendered image is not linked any more to the number of lens let in the micro array and it is possible to recover the full sensor resolution pushing it even to sub-pixel resolution [34, 35, 31]. This characteristic makes plenoptic systems suitable to a wider range of applications where high spatial resolution is required [6]. In the past years further effort has been made to push plenoptic 2.0 system to achieve super-resolution performances [58, 31, 29]. Here the term super-

resolution is not referred to the achievement of a resolution beyond diffraction limit[32] but to a digital sub pixel resolution only. Especially when applied to microscopy diffraction still is represents a big limitation for plenoptic imaging systems. In this chapter will be explained how diffraction affects the optical resolution of the imaging system and how it is linked to the spatio-angular trade off [19]. Numerical simulations will be used implemented by the platform described in chapter ??.

1.1 Rendering in Plenoptic 2.0

As introduced in chapter ??, rendering an image from plenoptic 2.0 raw data is based on integrating for each position all the correspondent directional coordinates. While in plenoptic 1.0 each position is sampled by a single lens let, that causes the loss of resolution in the final image, in plenoptic 2.0 each position is sampled by several lens lets. Therefore with reference to figure 1.1, the spatial coordinate (x,y) of point **A** will be sampled by the lens lets 1,2 and 3, therefore **A** is represented by 3 sub images. Each sub image is a different point of view of A and directional coordinates are sampled by these three points of view simultaneously. The number of sub images into which the point *A* is imaged depends by the magnification $m=b/a$ of the lens let array and is given by:

$$N_{sub} = \frac{1}{m} = \frac{a}{b} \quad (1.1)$$

a is the distance of the micro array from the main lens image and *b* is the distance of the from the sensor plane.

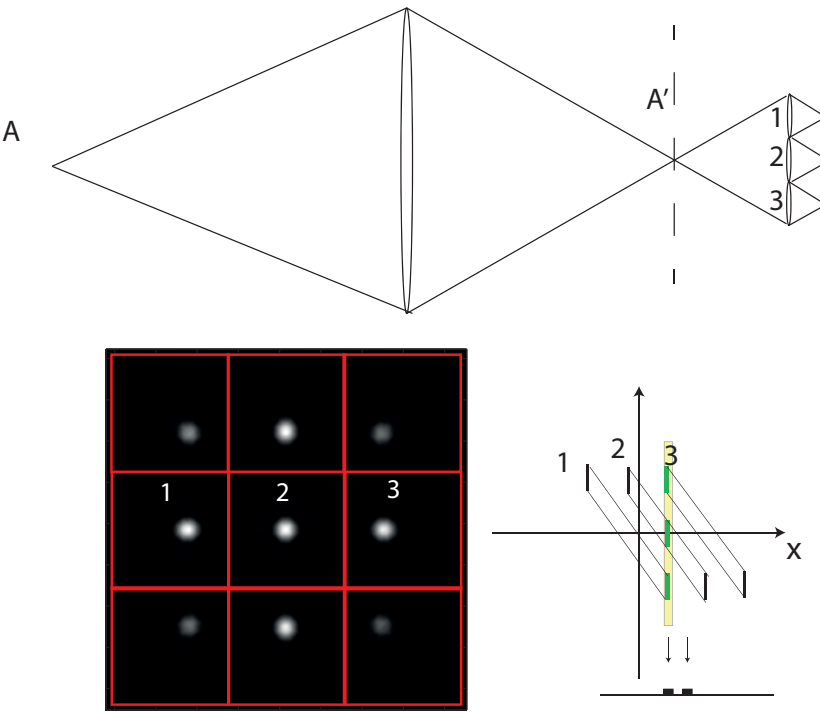


Figure 1.1: Top: the point **A** is imaged by the main lens into the point **A'**. **A'** is imaged by the lens let array into a number of sub images depending by the magnification of the micro array stage, in this case $m=0.333$. Bottom: particular of the raw image at the point source **A** and phase space diagram. The three sub images **1,2** and **3** are three different points of view of the object.

From a computational point of view the basic rendering is performed directly on the raw sensor image and has the following steps:

- the single sub images are isolated from each other
- depending on the magnification m the number of angular samples to be extracted from each sub image is calculated.
- the angular samples are extracted by the sub image and tiled all together forming the rendered image.

1.1.1 Extracting sub images

The effect of distortion must be taken into account when extracting the sub images from the raw data. The radial distortion is due to the fact that the sub images are shifted of certain amount because the lens lets are imaging off axis. The shift is proportional to the distance from the centre of the micro array [52] hence the effects of this distortion are larger on the sub images at the edges of the raw data sub images array. These result misaligned with respect to the regular square grid of the micro lens array. With reference to figure 1.2:

$$\frac{x}{z+a} = \frac{x'}{b} \quad (1.2)$$

Therefore each lens let is shifted of a quantity:

$$x' = \frac{xb}{z+a} \quad (1.3)$$

Since $z \approx z + a$ the centres of each sub image are shifted of a quantity equal to:

$$x' = x \frac{b}{z} \quad (1.4)$$

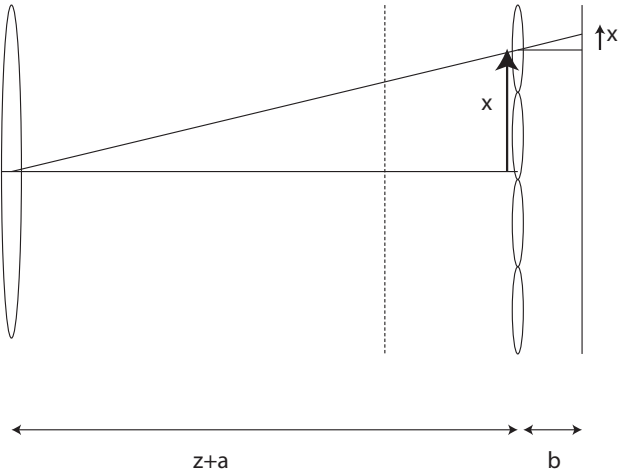


Figure 1.2: Relation between the position of the centre of a lens let x and the position of the centre of the correspondent sub image $x + x'$.

In figure 1.2 x is the position of the centre of a micro lens and its corresponding sub image will be shifted of a quantity x' . on the distance of the image plane from the main lens z and the distance of the sensor form the micro lens b . Once the centres of the sub images have been localized it is possible to extract each sub image of them from the raw data and perform the rendering.

1.1.2 Basic Rendering

This section will describe how the basic rendering algorithm works as seen in section ?? and as described by Georgiev and Lumsdaine [3, 35] . The raw image on the sensor plane is an image of the main lens image plane [3]. Each sub image represents a single point of view of an area of the main lens image plane. Referring to figure 1.3, if the micro array is composed by N x N lens lets, the raw sensor image will be composed by an N by N array of sub-images. Each sub-image has a dimension of $P \times P$ where P is the micro

lens pitch.

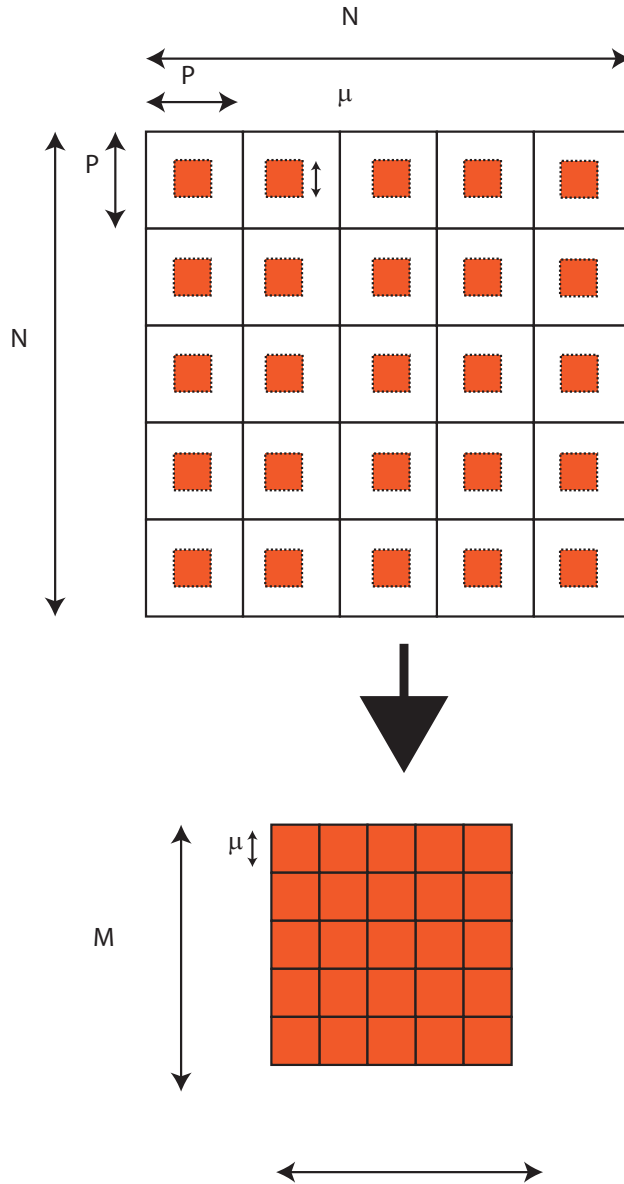


Figure 1.3: Basic rendering algorithm. The Rendered image is composed tiling together patches extracted by each sub image. The patch size is dependent by the magnification of the micro array stage.

The magnification of the micro array is $m=b/a$ and each micro lens maps the main lens image on the sensor plane on a sub image magnified of a quan-

tity m . Therefore from each sub image a patch is selected with a dimension equal to:

$$\mu = P \frac{b}{a} = Pm \quad (1.5)$$

The patch size depends on the magnification of the lens lets array. The next section will be shown how this fact can be used to recover depth information from the raw sensor images.

1.1.3 Depth based rendering

The patch size μ as seen in equation 1.5 depends on the magnification of the micro array stage. If the point imaged is out of focus, its image will be formed on a different plane that is not the main lens image plane. Hence the main lens image will be blurred and so will be the sub images on the sensor. If during the rendering process is taken into account that a point at a different depth with respect to the main lens focal plane will be imaged at a different distance from the micro lens array, it is possible to define a new value of magnification m' to which will correspond a new patch size μ' . With reference to figure 1.4, the points that belong to the plane shown represented by the dashed red line placed at a distance d from the object plane, will be imaged on a plane in between the main lens and the main lens image plane. It is possible to define a virtual micro array stage with respect to this plane for which its points will be imaged in focused on a virtual sensor plane. The parameters characterizing the virtual micro array stage are the distances a' and b' and a magnification $m' = b'/a'$.

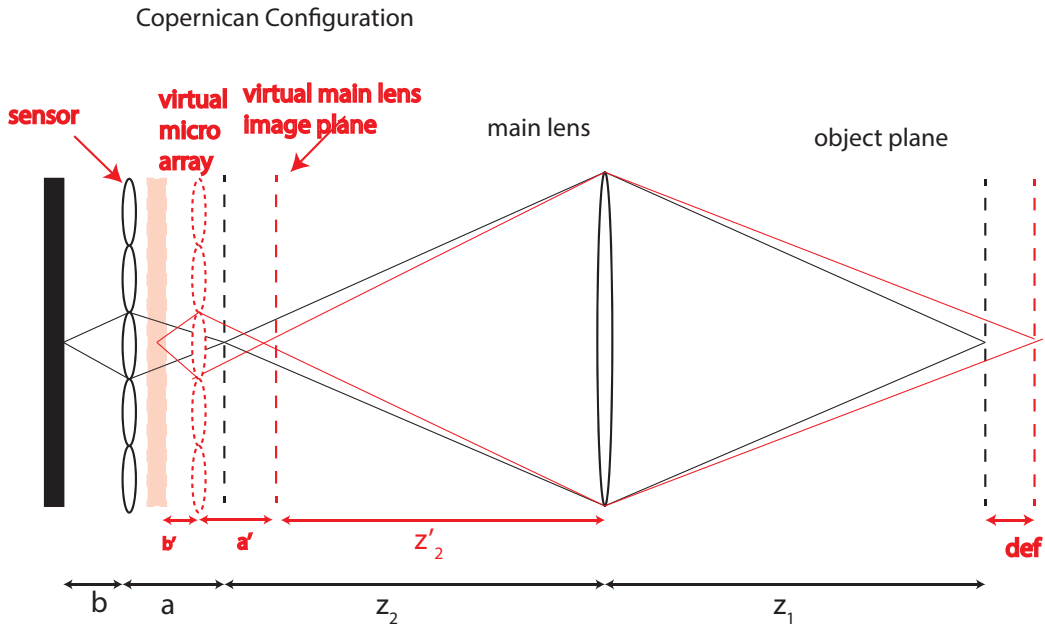


Figure 1.4: The points that belongs to the object plane represented in red are imaged on a virtual main lens image plane. This plane is relayed on a virtual sensor plane by a virtual micro array whose parameters are a' and b' and $m' = b'/a'$.

The distance between the main lens image plane and the virtual main lens image plane, defined as $\alpha = a - a'$, is called virtual depth [59]. It is linked to the actual defocus of the object plane by the lens law referred to the main lens. The magnification of the virtual lens let array defines the patch size to use to rendered the point at that particular depth. The link between the magnification m' and m can be defined by applying twice the lens law, once for the main lens and once for the micro array stage. Therefore the virtual main lens plane corresponding to a defocus d is located at:

$$z'_2 = \frac{(z_1 + d)f}{(z_1 + d) + f} \quad (1.6)$$

f is the focal length of the main lens. The corresponding virtual depth value

is given subtracting the quantities z'_2 and z_2

$$\alpha = z'_2 - z_2 \quad (1.7)$$

Then from the virtual depth α the values a' and b' for the virtual micro array can be obtained.

$$\begin{cases} a' = a - \alpha \\ b' = \frac{a'f}{a' + f} \end{cases} \quad (1.8)$$

And the magnification for the virtual plane is:

$$m' = \frac{b'}{a'} \quad (1.9)$$

Values of the magnification m' plotted as a function of defocus are shown in figure 1.5

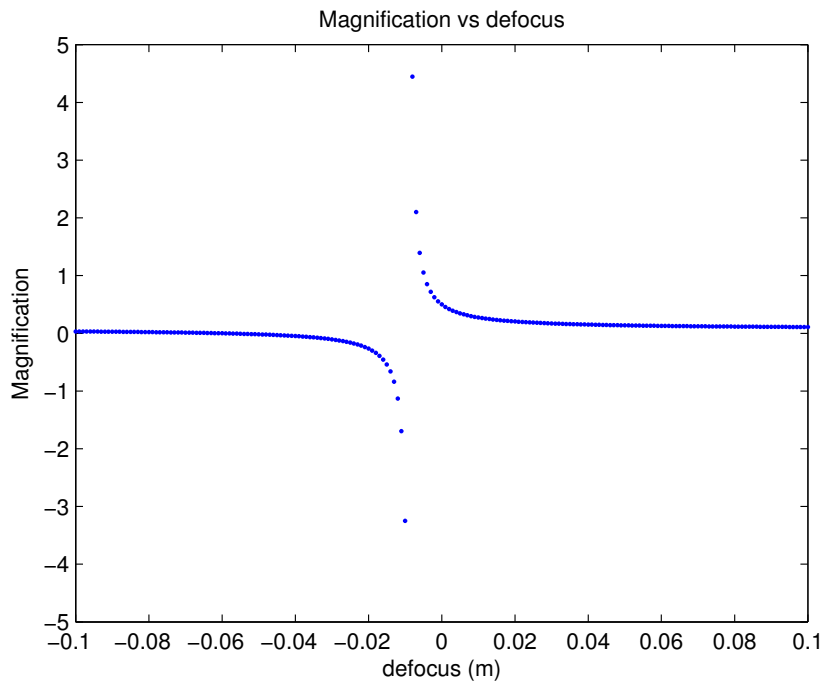


Figure 1.5: .

The patch size corresponding to the new focal plane is therefore:

$$\mu' = Pm' = P \frac{b'}{a'} \quad (1.10)$$

Rendering with the new patch size allows to refocus at a different plane. If the defocus is not known, as it happens in the majority of the cases, is it possible to estimate the depth information of the scene imaged and using this information to render the final image. This algorithms are based on cross correlating each sub image with its closest neighbours in order to evaluate the relative shift due to a change in depth across the lens let[60, 61]. In this way it is possible to determine the patch size that results in the best match with all of its neighbours [3, 34]. The axial resolution of a plenoptic 2.0 system is determined by considering that the minimum shift between neighbouring lens lets is the one equal to one pixel.

1.2 Description of the system

The system simulated is shown in figure 1.6. The main lens is in a 2f configuration, therefore $z_1 = z_2 = z$.

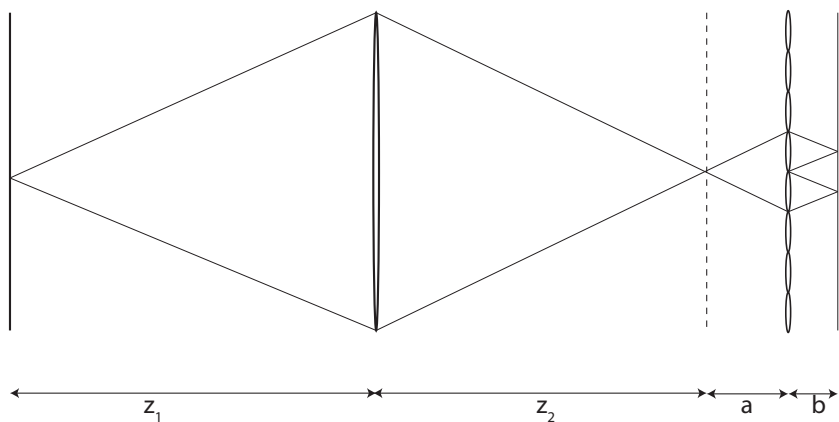


Figure 1.6: Ray diagram of the system simulated.

The main objective of the simulation on a plenoptic 2.0 system was to investigate its behaviour at diffraction limit as well as to better understand the trade-offs in resolution and how the different parameters of the systems affects it. Different combinations of the optical parameters of the system, including main lens aperture, micro array pitch and magnification, have been tested. The modularity of the Fresnel simulation toolbox allows to easily change the simulation parameters independently and collect results. The system parameters are defined; these are the dimension and the number of pixel on the sensor, the pitch and focal length of the lens let array, the focal length of the main lens and the magnification m aof the micro array stage. The the simulation toolbox is capable of automatically setting all other simulation parameters to respect the f-number matching between the main lens and the lens let array. In a plenoptic 2.0 imaging system the f-number is matched when:

$$\frac{z_2}{d} = \frac{b}{p} \quad (1.11)$$

If the lens let array has a focal length equal to f_μ and a pitch equal to p , the value of the distance from the sensor b can is obtained by the magnification m as:

$$b = m f_\mu \left(1 + \frac{1}{m} \right) \quad (1.12)$$

Equation 1.12 has been obtained substituting the expression of the magnification $m = b/a$ into the lens equation $1/a + 1/b = 1/f_\mu$. Values of the parameter b as a function of the magnification can be seen plotted in figure 1.7

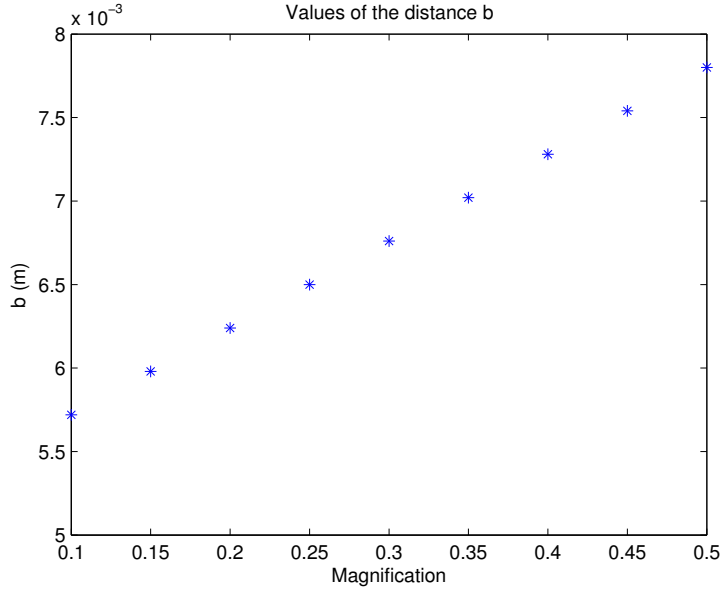


Figure 1.7: Values of the parameter b correspondent to values of magnification varying from 0.1 to 0.5.

Once b is defined the distance of the micro lens array from the main lens image is calculated by solving the lens law for a :

$$a = \frac{bf}{b-f} \quad (1.13)$$

Values of a as a function of the magnification can be seen in figure 1.8:

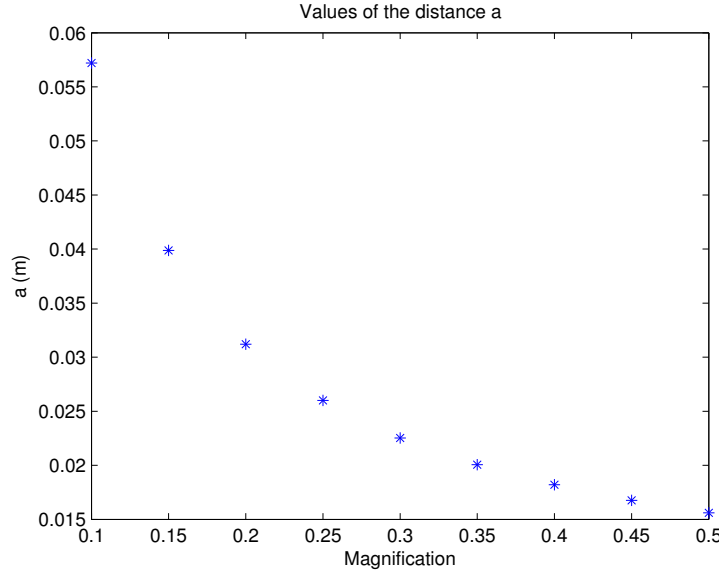


Figure 1.8: Values of the parameter b corresponding to values of magnification varying from 0.1 to 0.5.

Now that the relay system has been defined, the software defines the aperture of the main lens matching its f-number to the one of the lens let using equation 1.11. We have:

$$r_{lens} = \frac{zp}{2b} \quad (1.14)$$

Values of a as a function of the magnification can be seen in figure

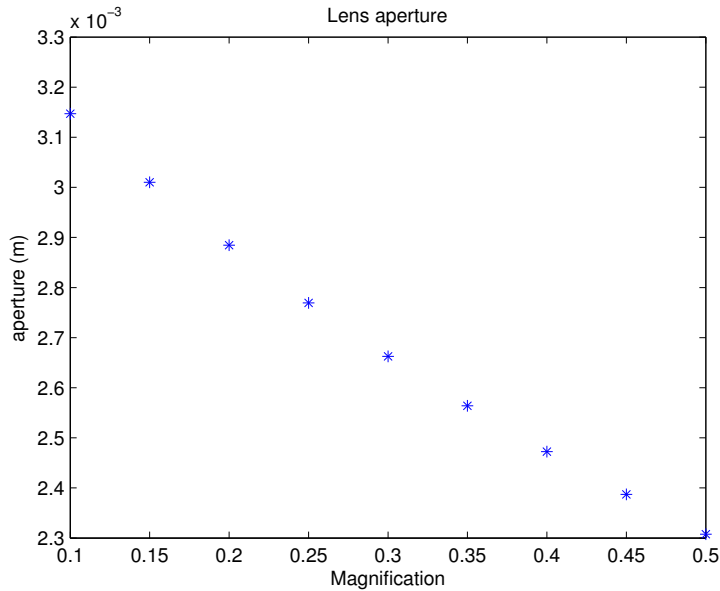


Figure 1.9: Aperture of the main lens as a function of the magnification in order to respect the f-number matching condition.

Therefore the simulation platform is able to set the simulations parameters when some other are given, making the launching procedure of each simulation easy and quick. We set the micro lens array with the following characteristic:

Array size	5.8 x 5.8 mm
Micro lens focal length f_μ	5.3 mm
Micro array pitch p	150 μm
sensor size	5.8 x 5.8 mm
sensor resolution	3500 by 3500 pixel
pixel size	1.67 μm
number of lens let	39 x 39 lens lets
main lens focal length	60 mm

And the values obtained for a, b and the main lens aperture corresponding to the magnification investigated are:

Magnification	<i>a</i>	<i>b</i>	main lens aperture
0.5	15.6 mm	7.8 mm	2.3 mm
0.3	22.5 mm	6.8 mm	2.7 mm
0.25	26 mm	6.5 mm	2.8 mm

1.3 Optical performances of a focused plenoptic system

This section shows the results obtained running simulations of the system described in section 1.2 at its diffraction limit. Three different configurations of the micro lens array stage have been tested, corresponding to the parameters a and b set in order to have magnification $m = b/a$ equal to 0.5, 0.3 and 0.25. The first simulation presented is the image of a single focused point source. A comparison between the main lens image and the rendered image will be done to understand the differences in optical resolution and to evaluate the noise induced by the rendering algorithm. The optical resolution of an imaging system is defined by its impulse response, known as point spread function [47, 52]. If the input is a point source in focus, the output image for an unaberrated circular aperture has a well known intensity profile, the Airy disk. The Airy disk defines the broadening that a point source undergo after being imaged by an optical system, hence it is a good estimation of the minimum feature resolvable by the system [47, 62]. The Airy disk is shown in figure 1.10. The position of the first zero of the Airy disk is given by:

$$x_1 = 1.22\lambda F_\# \quad (1.15)$$

and the total extension of the central lobe is defined as the distance between the first two zeros as:

$$\Delta x = 2.44\lambda F_\# = 2.44\lambda \frac{b}{p} \quad (1.16)$$

where λ is the wavelength of the radiation, b is the distance between the lens let and the sensor and p is the pitch of the micro array and the aperture of the single lens let. The central lobe contains the 90% of the total energy of the optical field, therefore its extension defines the spread that each point undergoes in the final image.

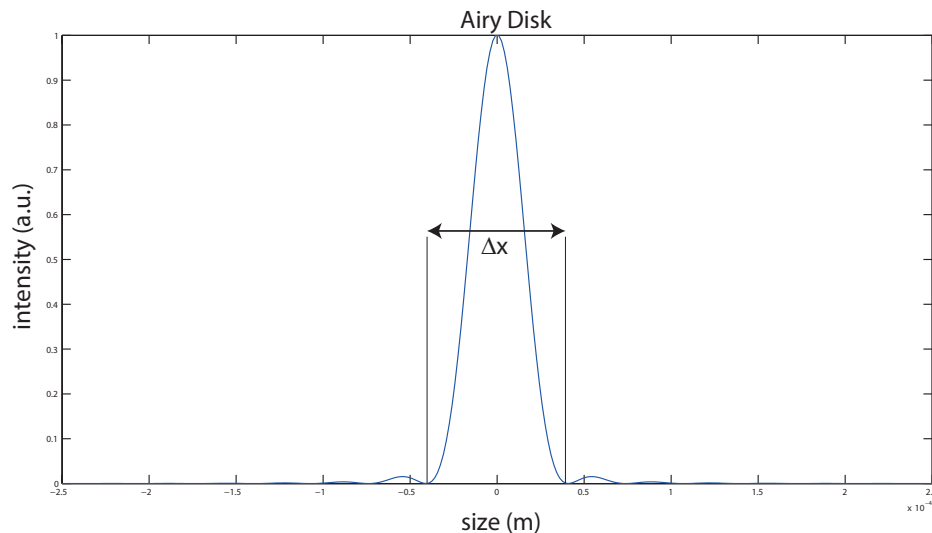


Figure 1.10: Aperture of the main lens as a function of the magnification in order to respect the f-number matching condition.

We define Δx is the optical resolution of the imaging system. In a plenoptic 2.0 system there are two elements that influence the optical resolution, the main lens and the micro lens array. Because of the f-number matching condition, the optical resolution in the two imaging stages should be the same. But because of the magnification present in the micro array stage,

which is different from the magnification of the main lens, the coordinates in the main lens image plane are rescaled by a factor equal to the magnification m when imaged by the micro array on the sensor [47]. Using the coordinates x' and y' of the main lens image plane, the sub image coordinates will be given by:

$$\begin{cases} x = \frac{x'}{m} \\ y = \frac{y'}{m} \end{cases} \quad (1.17)$$

Therefore if a pixel on the main lens image samples a feature size of δx , on the sensor the same pixel will sample a quantity $\delta x/m$. Because m is smaller than 1, the spread of a point on the sensor plane will be bigger than the one on the main lens image plane. The same pixel samples a bigger area of the object in the image. This leads to a loss in optical resolution [20]. The smaller is the magnification, the broader becomes the point spread function and as a consequence the band pass of the micro lens array becomes narrower.

The optical cut off frequency is defined as:

$$\nu_{cutoff} = m \frac{1}{\lambda f_\#} = m \frac{b}{\lambda p} \quad (1.18)$$

Figure 1.11 shows the values of the lateral resolution plotted in function of the magnification of the micro array stage, while in figure 1.12 are plotted the correspondent values of the optical cut off frequency.

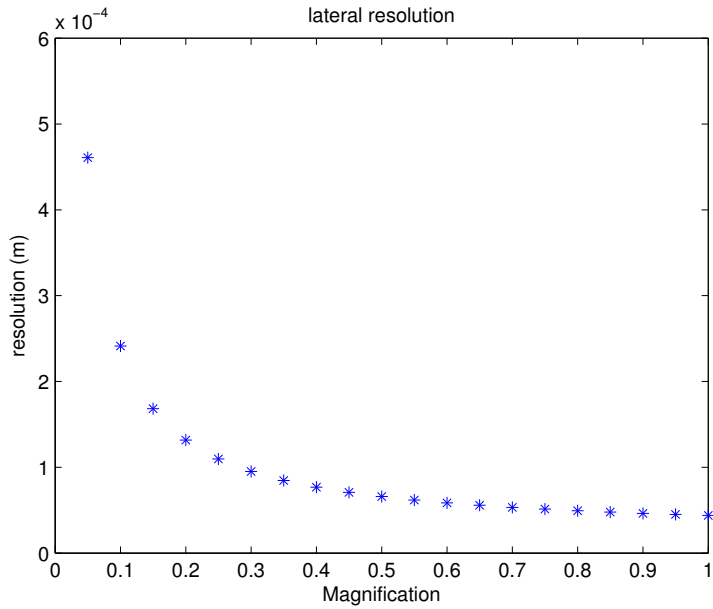


Figure 1.11: lateral resolution as a function of the magnification.

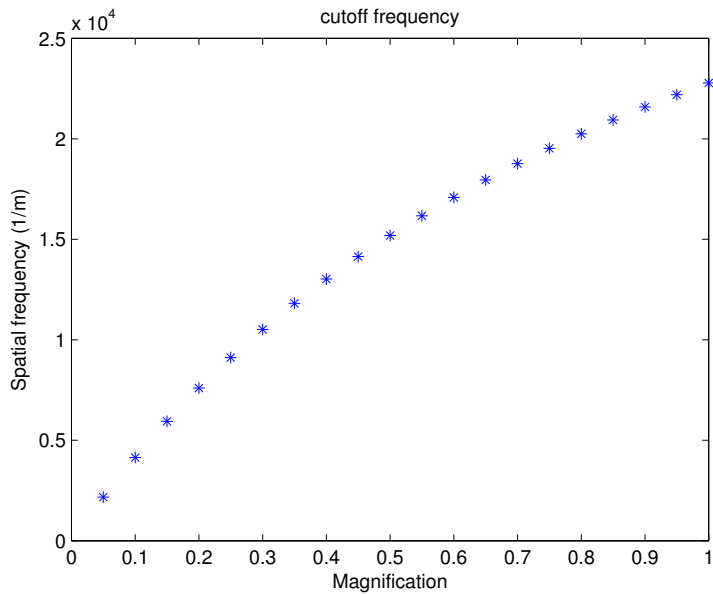


Figure 1.12: optical cut-off frequency as a function of the magnification.

This means that in a plenoptic 2.0 imaging system exists an intrinsic trade-off between optical resolution and spatio-angular resolution. The trade

off between spatial and angular resolution has been described in section ??.

A further trade off is now present and is it due to diffraction. A low magnification allows to sample very well the direction and therefore to have a finer axial resolution when evaluating depth but a magnification too low will filter out high frequency components of the object. In the next sections will be investigate in detail the optical performances of a focused plenoptic system, performing simulations to better understand the trade off between spatio-angular resolution and optical resolution. This is the first attempt of evaluating the effects of the optical parameters of a focused plenoptic system on the the optical resolution using a wave optics approach.

1.4 Impulse response of a Focused Plenoptic system

The first simulation performed was designed to obtain the impulse response of a focused plenoptic system. The point source has been simulated using a pupil with a diameter of $10 \mu m$. As explained in section 1.1, the magnification gives the number of points of view that sample an image. To have directional information, a point of the object should be sampled at least by two point of view, therefore by two lets. In this way two set of directional coordinates are captured and on the sensor and each point repeated four times on the raw image, two times horizontally and two vertically. With a magnification of 0.5, the sub images will be 2 per direction, with a magnification of 0.3 each point is expected to be replicated 3 times, and with a magnification of 0.25 four times. Figures 1.13 , 1.14 , and 1.15 show the raw sensor images and the rendered images of a point source when the magnification is 0.5, 0.3 and

0.25.

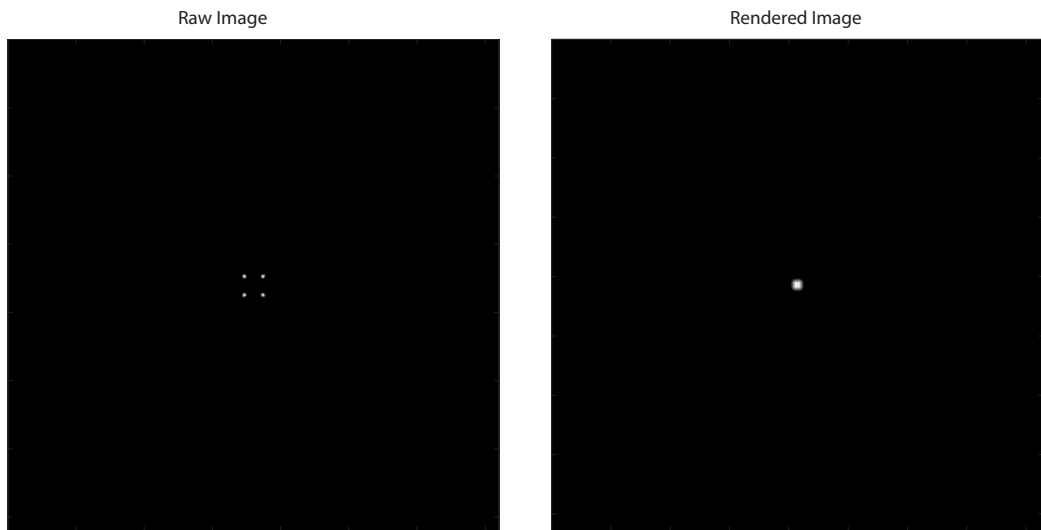


Figure 1.13: Left: raw sensor image, Right: rendered image. Artifacts are present. Magnification: 0.5

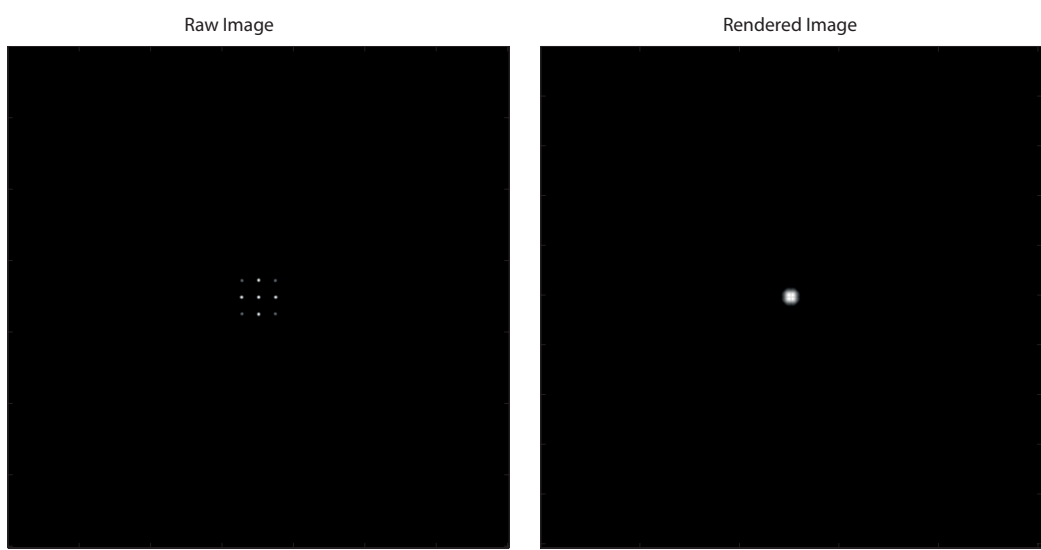


Figure 1.14: Left: raw sensor image, Right: rendered image. Artifacts are present. Magnification: 0.3.

1.4. IMPULSE RESPONSE OF A FOCUSED PLENOPTIC SYSTEM 21

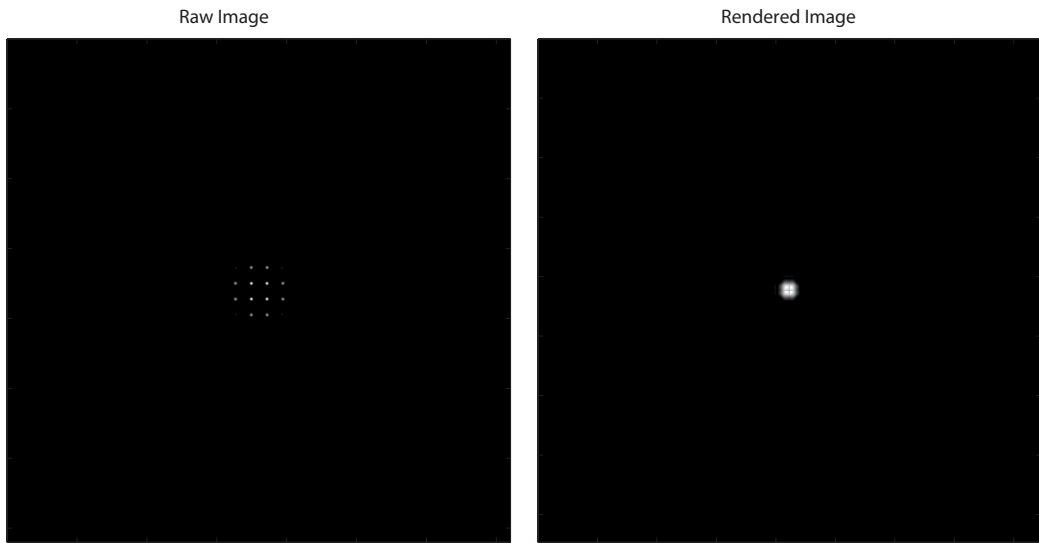


Figure 1.15: Left: raw sensor image, Right: rendered image. Artefacts are present. Magnification: 0.25

Figure 1.16 shows the intensity profiles of the main lens image and of the rendered images. The profiles are obtained by sum all the rows of the matrix of the image and normalizing by its.

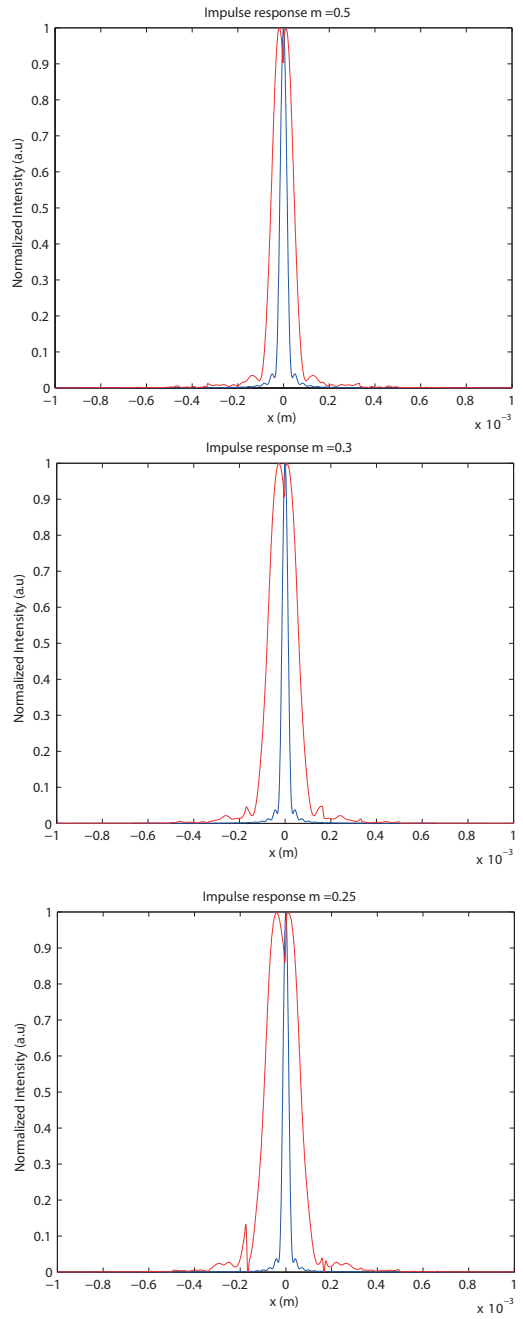


Figure 1.16: From top to bottom: comparison between the main lens image profile, in blue, and the rendered image profile, in red, for magnification values of 0.5, 0.3 and 0.25. The central lobe of the rendered image increase with the magnification, as well as the number of artefacts.

From figure 1.16 it is possible to appreciate the broadening effects of the central lobe of the rendered image intensity profile, in red, with respect to the main lens image. The central lobe size is also dependent on the magnification used as seen in figure 1.11. With a small magnification, the number of sub images that sample a single point source increase, and due to the nature of the rendering process explained in section 1.1.2, the number of artefacts increases, broadening the central lobe and making the lateral resolution worse. Table 1.4 shows the values of the central lobe size of the main lens image, Δx , of the rendered image $\Delta x'$ and the ratio between them. Error in the ratio is due to the presence of artefacts generated by the rendering algorithm that increases with the decrease of the magnification.

Magnification	Δx (m)	$\Delta x'$ (m)	$\Delta x/\Delta x'$
0.5	7.848×10^{-5}	2×10^{-4}	0.392
0.3	6.848×10^{-5}	2.698×10^{-4}	0.25
0.25	6.514×10^{-5}	3.574×10^{-4}	0.18

1.5 Two point resolution

Another important instrument to evaluate the resolution of an imaging system is the Rayleigh criterion of resolution. It states that two incoherent point sources are resolved by a diffraction limited imaging system when the centre of the Airy disk intensity pattern generated by one point source falls exactly on the first zero of the Airy disk generated by the other point source [47]. The Rayleigh criterion of resolution states that for two point source of light whose relative phase differs for $\pi/2$ the minimum distance to resolve them

both in the image plane is given by:

$$\delta x = 1.22\lambda \frac{z}{d} \quad (1.19)$$

Where d is the lens aperture and z is the propagation distance. In the simulation the two point sources were placed at distance equal to the Rayleigh distance and they have been imaged by a plenoptic 2.0 system where the micro lens array had a magnification of 0.5. The purpose of this experiment is to prove that the magnification of the micro lenses gives a limits the optical resolution of the system. Figure 1.17 shows the main lens image and the rendered image with their respective intensity profiles, of two point source with a diameter of $10 \mu m$ separated by a distance $\delta x = 40\mu m$. The imaging system simulated is the same described in section 1.2.

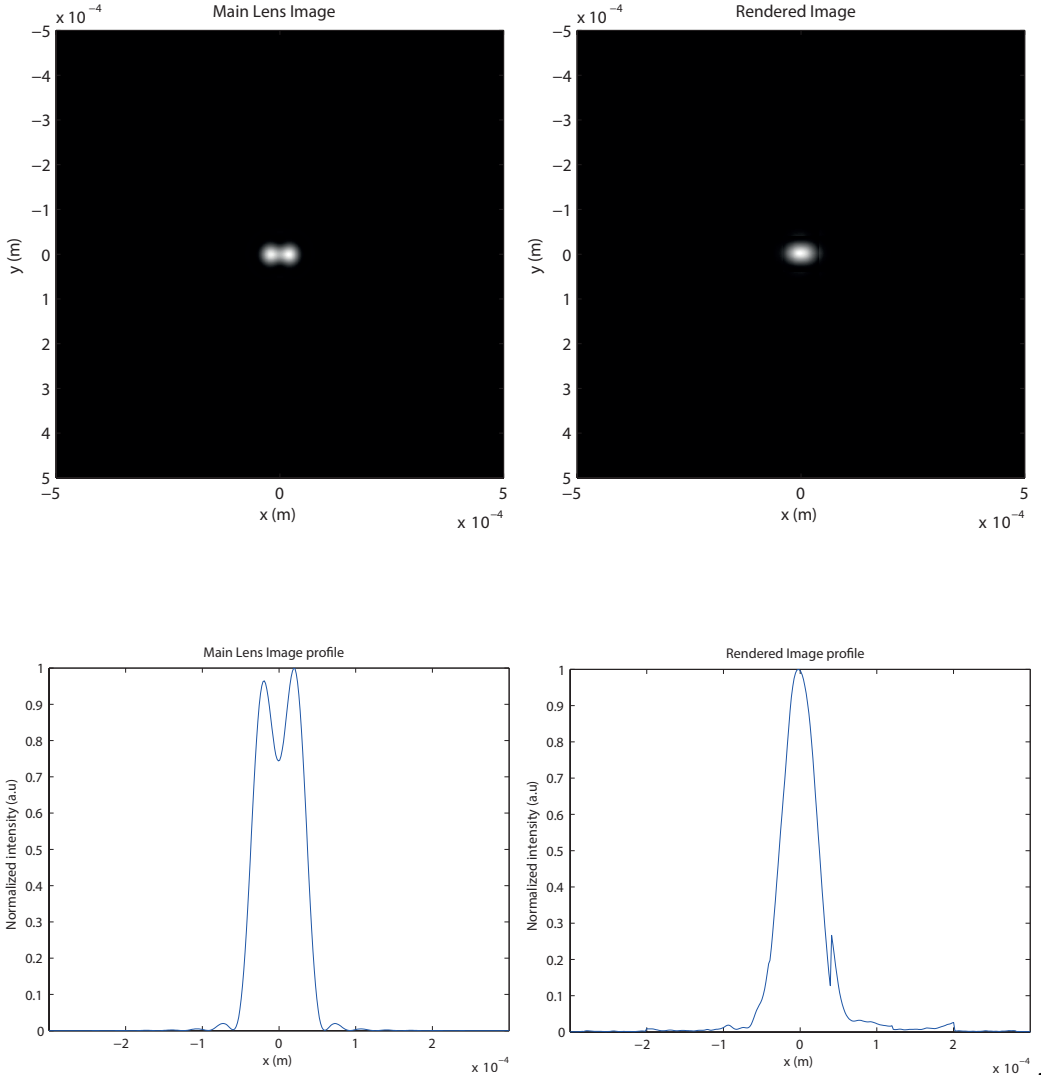


Figure 1.17: On the top left there is the main lens image of two point sources separated by the Rayleigh distance δx . On the top right its corresponded rendered plenoptic image obtained with a magnification of 0.5. As expected from the theory, the resolution of the rendered image is half the one of the main lens image, and the two points are no more distinguishable as confirmed by the intensity profiles of the two images on the bottom.

While in the main lens image the two point sources are at the limit of resolution and the two points are still resolvable, in the rendered image the two spot sizes are merged together and no longer resolvable. If the

separation between the point sources is doubled in the object plane they should be resolve in the rendered image too while keeping the magnification 0.5. Figure 1.18 shows the simulations results for a $\delta x = 80\mu m$:

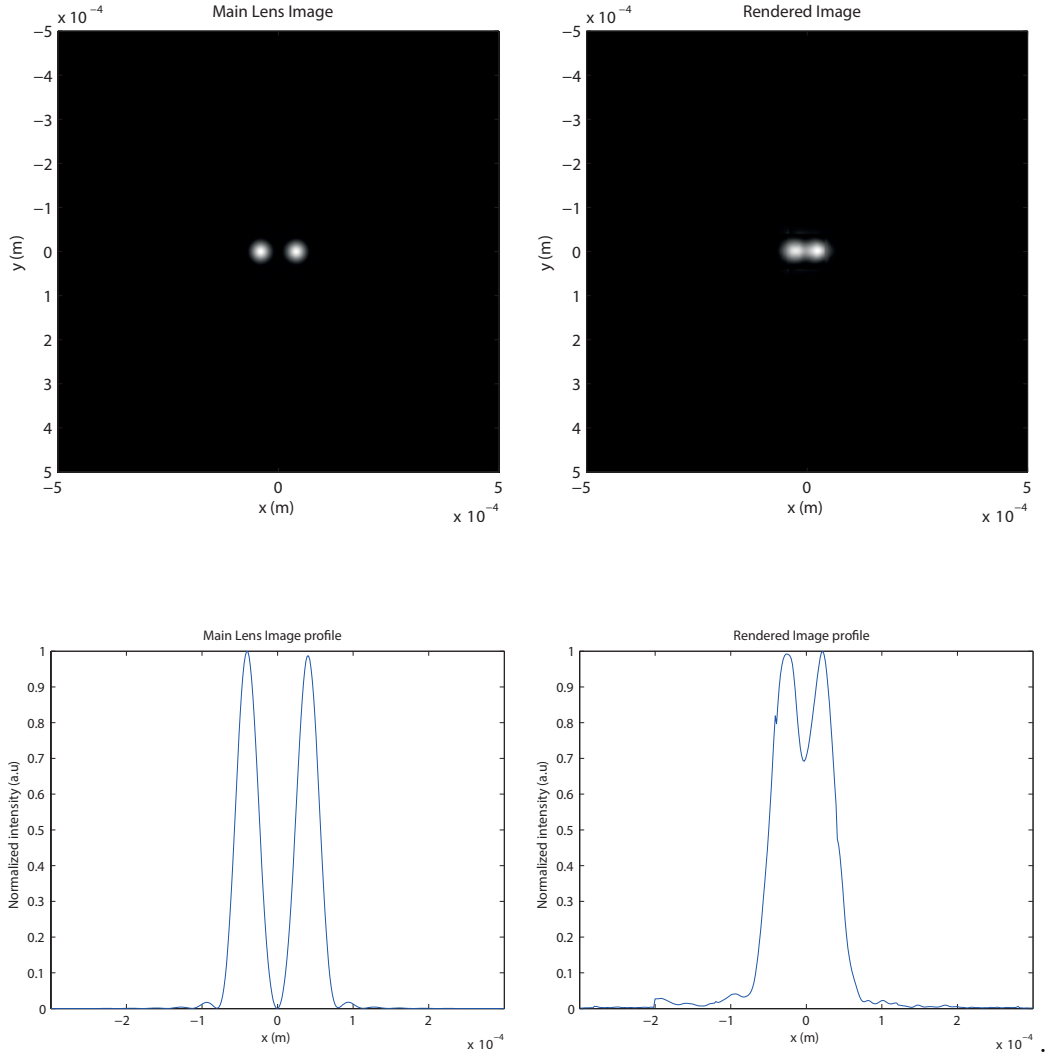


Figure 1.18: The image on the top left shows the main lens image of two point sources separated by the Rayleigh distance $2\delta x$. On the top right there is its corresponded rendered plenoptic image obtained with a magnification of 0.5. Doubling the Rayleigh distance the rendered image is at the limit of resolution, where the maximum of the Airy pattern of one point falls on the first zero of the second point.

This results obtained simulating wave optics propagation in the plenoptic imaging system confirm the predictions made in section 1.3 and it is the first experiment of this kind. When imaging an object with a plenoptic 2.0 system the loss of resolution due to the magnification should be taken into account in order not to lose useful information in the sample, or a suitable lens let array configuration should be chosen.

1.6 Frequency analysis of a focused plenoptic system

This section will describe the frequency response of a focused plenoptic system and its dependency on the magnification of the lens let array stage. The spatial frequencies that are transferred from the object to the image plane in an optical system are defined by its modulation transfer function (MTF). The MTF is defined as the square modulus of the Fourier transform of the impulse response $h(x,y)$ of an optical system [47].

It is then:

$$H(f_x, f_y) = |\mathcal{F}\{h(x, y)\}| \quad (1.20)$$

It represents the weighting factor applied by the system to all the frequency components of the optical field coming from the object. The visibility and the contrast of the points corresponding to the different values of spatial frequency changes according to the modulation imposed by the MTF. When it goes to zero, no energy is transmitted for that particular frequency and the detail is no longer present in the image. The value of spatial frequency for which the MTF goes to zero is called optical cut-off frequency. In this section

the effects of the magnification on the location of optical cut-off frequency is investigated. The first result presented is obtained by calculating the modulation transfer function of the plenoptic 2.0 system described in section 1.4, with magnification values of 0.5, 0.3 and 0.25. The MTF for these three cases are shown in figure ??, ?? and ?? and have been obtained applying equation 1.20 to the intensity profiles in figure 1.16. In all the three figures, in green is shown MTF of the single lens imaging system, without the lenslet array stage, and in red the MTF of the plenoptic system.

1.6. FREQUENCY ANALYSIS OF A FOCUSED PLENOPTIC SYSTEM 29

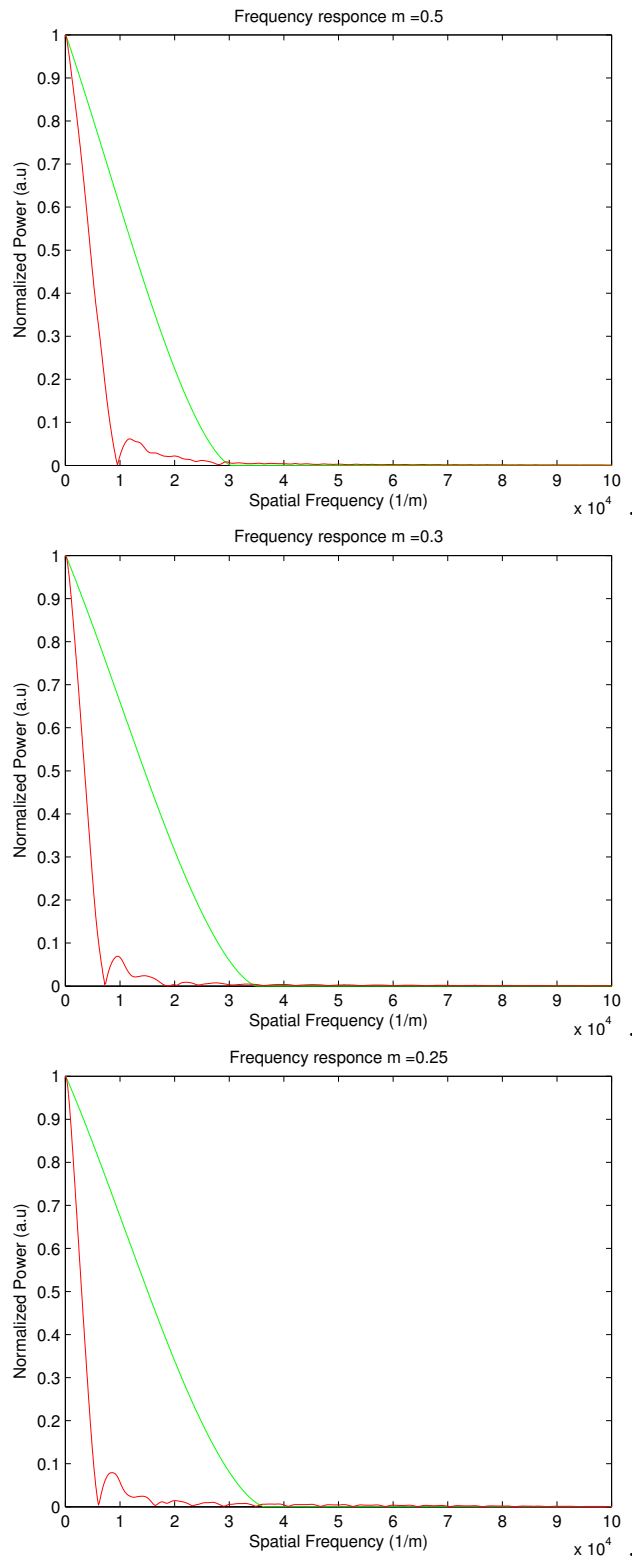


Figure 1.19: Modulation transfer functions of the main lens (green) and the overall imaging system (red) for a magnification value of $m = 0.5$, top, $m = 0.3$, central, and $m = 0.25$, bottom.

From figure 1.19 it is possible to see that the cut off frequency of the single lens system increases with the decreasing of the magnification, while the cut-off frequency decrease with the decreasing of the magnification if the lens let array stage is added. This result is in accord with what seen in sections 1.3 and is a direct consequence of the simulations results shown in section 1.4. The magnification of the micro lens array reduces the optical resolution. this is a direct consequence of the intrinsic trade-of between optical resolution and the spatio-angular resolution. While reducing the magnification of the micro array stage increase the number of directional samples, at the same time makes the optical bandwidth narrower, reducing the lateral resolution. The decrease in the optical cut-off frequency is directly proportional to the decrease of the magnification as predicted in the theory with equation 1.18 and proved by the numerical simulation. This effect will be observed in the images obtained by the real system described in chapter 1). The values of the cut-off frequencies obtained by the simulations are:

Magnification	Rendered $f_{cut-off} m^{-1}$	Main lens $f_{cut-off} m^{-1}$
0.5	1.00×10^4	3.00×10^4
0.3	0.76×10^4	3.50×10^4
0.25	0.63×10^4	3.60×10^4

The second set of simulations done evaluates the effects of the magnification in more detail. A varying frequency sinusoidal grating is imaged incoherently, as explained in chapter ??, by the system with the same three different configurations of the micro array stage. The Grating contains five different frequencies :

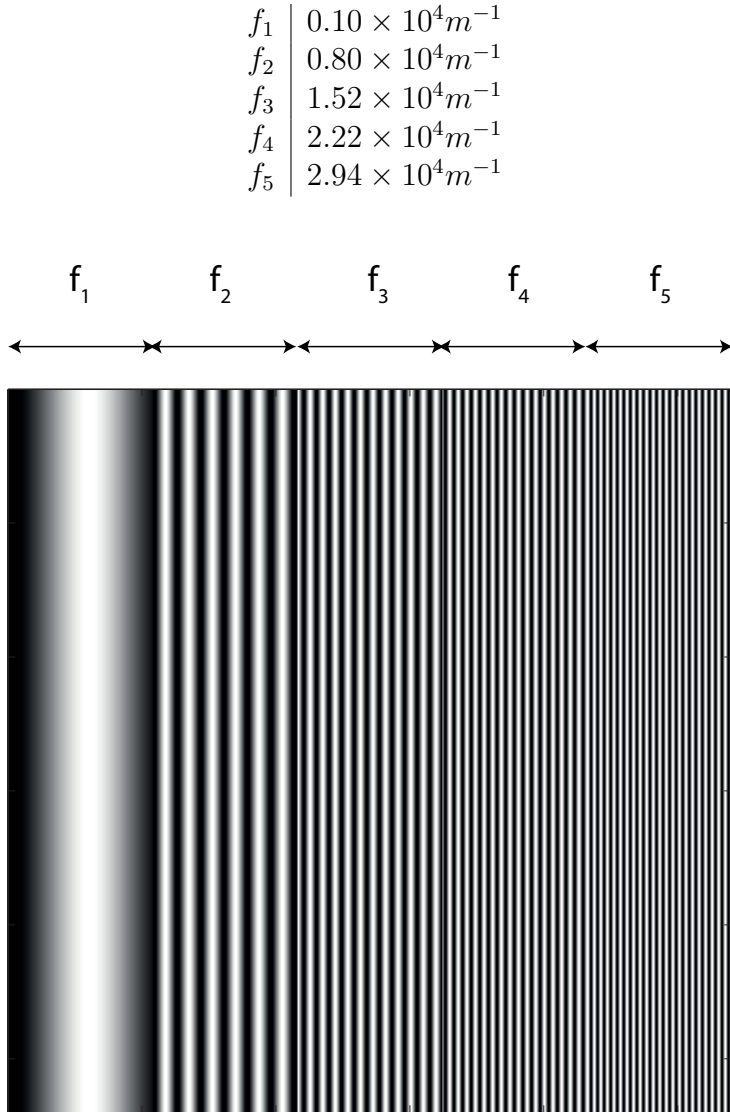


Figure 1.20: The object imaged in this simulation is a sinusoidal grating containing five different frequencies.

Figure 1.21 shows the raw image, the main lens image and rendered images of the sinusoidal grating shown in figure 1.20, imaged with a magnification of $m = 0.5$. The two rendered images are obtained with the basic rendering explained in section 1.1. To remove digital artefacts given by the tiling of the sub images patches on the rendered images a low pass Gaussian filter with

$\sigma = 1.162 \times 10^4$ has been applied.

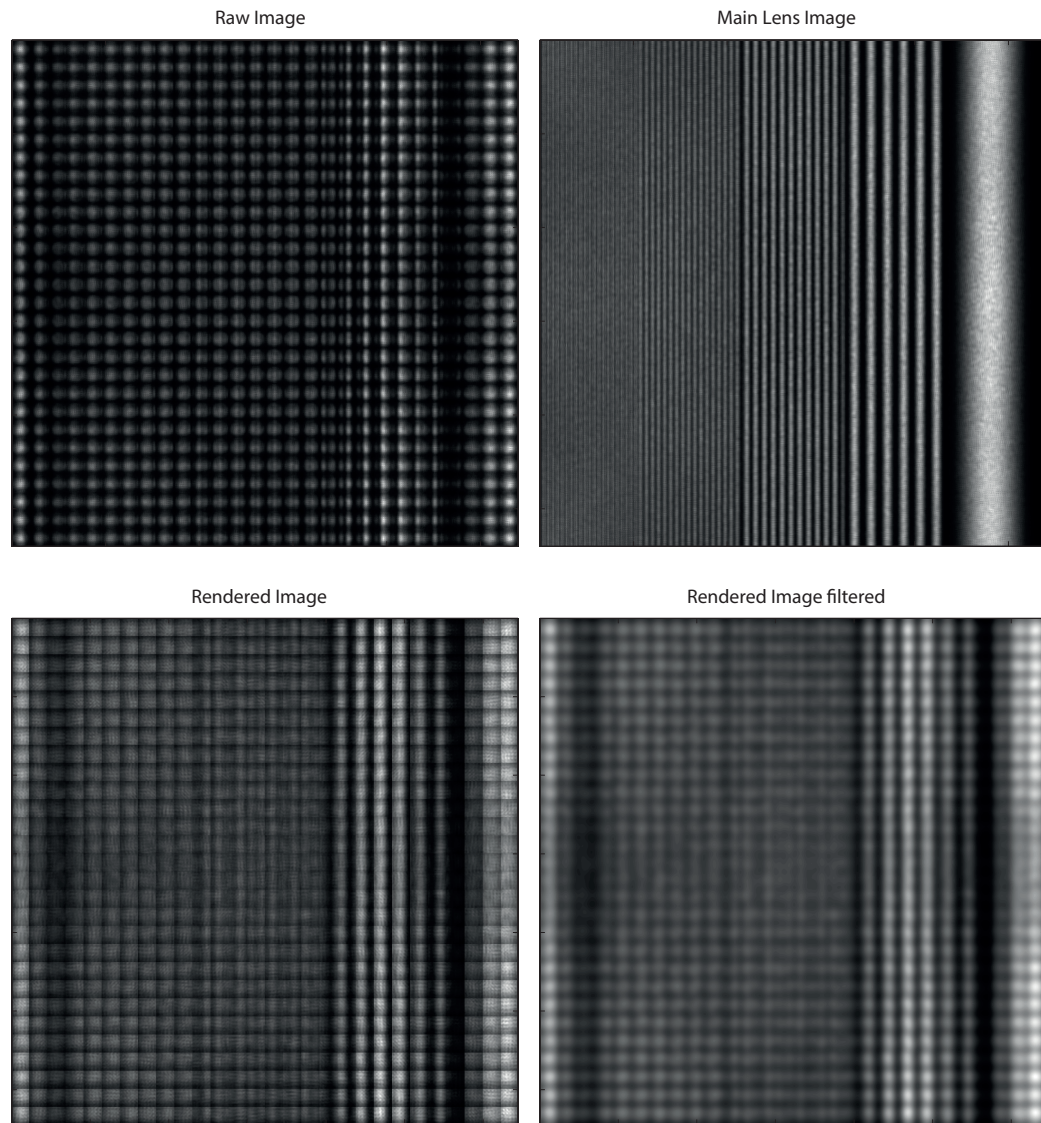


Figure 1.21: Top: on the left it is shown the raw sensor image, on the right the main lens image. Bottom: On the left there is the rendered image, on the right the same image has been low pass filtered to remove some of the rendering artefacts. Magnification was 0.5

The normalized intensity profile of the optical field at the main lens image plane compared with the intensity profile of the rendered image is shown in

1.6. FREQUENCY ANALYSIS OF A FOCUSED PLENOPTIC SYSTEM 33

figure 1.22 on the left side while on the right the power spectra of the main lens image and of the rendered image is presented. The modulation transfer function of the main lens and of the full plenoptic system has been added in red.

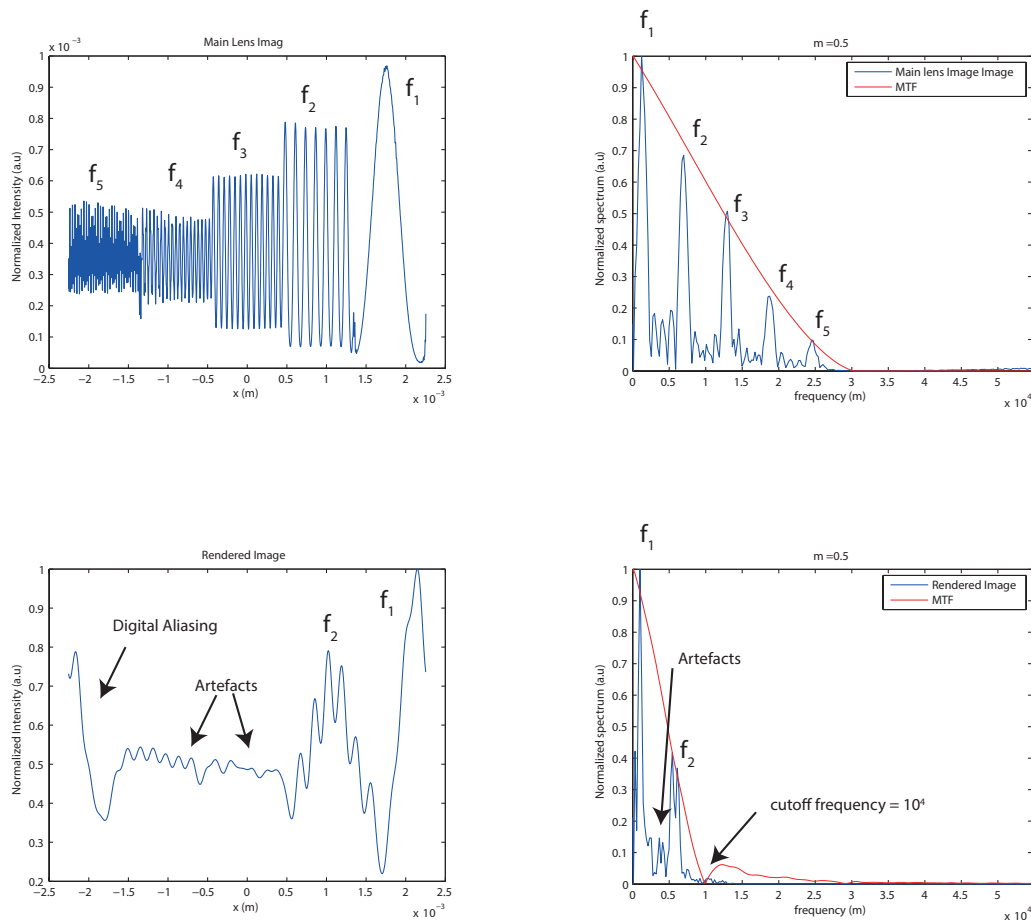


Figure 1.22: On the left: intensity profiles of the main lens image, top and of the rendered image, bottom. On the right the spatial frequencies modulated according to the MTF as shown by the power spectra of the main lens image on the top right and of the rendered image on the bottom right. The magnification of the lens let array is $m = 0,5$ and cut-off frequency of the system is $f_{cut-off} = 10^4 m - 1$

As expected the amplitude of the oscillations in both the main lens image and the rendered image follow the profile of the modulation transfer function of the two stages. Not all the frequency components of the object field are transmitted through the different stages of the plenoptic imaging system. In fact it acts as a low pass filter, whose bandwidth depends on the magnification used in the lens let array stage. The low pass filtering action is shown in figure 1.23.

1.6. FREQUENCY ANALYSIS OF A FOCUSED PLENOPTIC SYSTEM 35

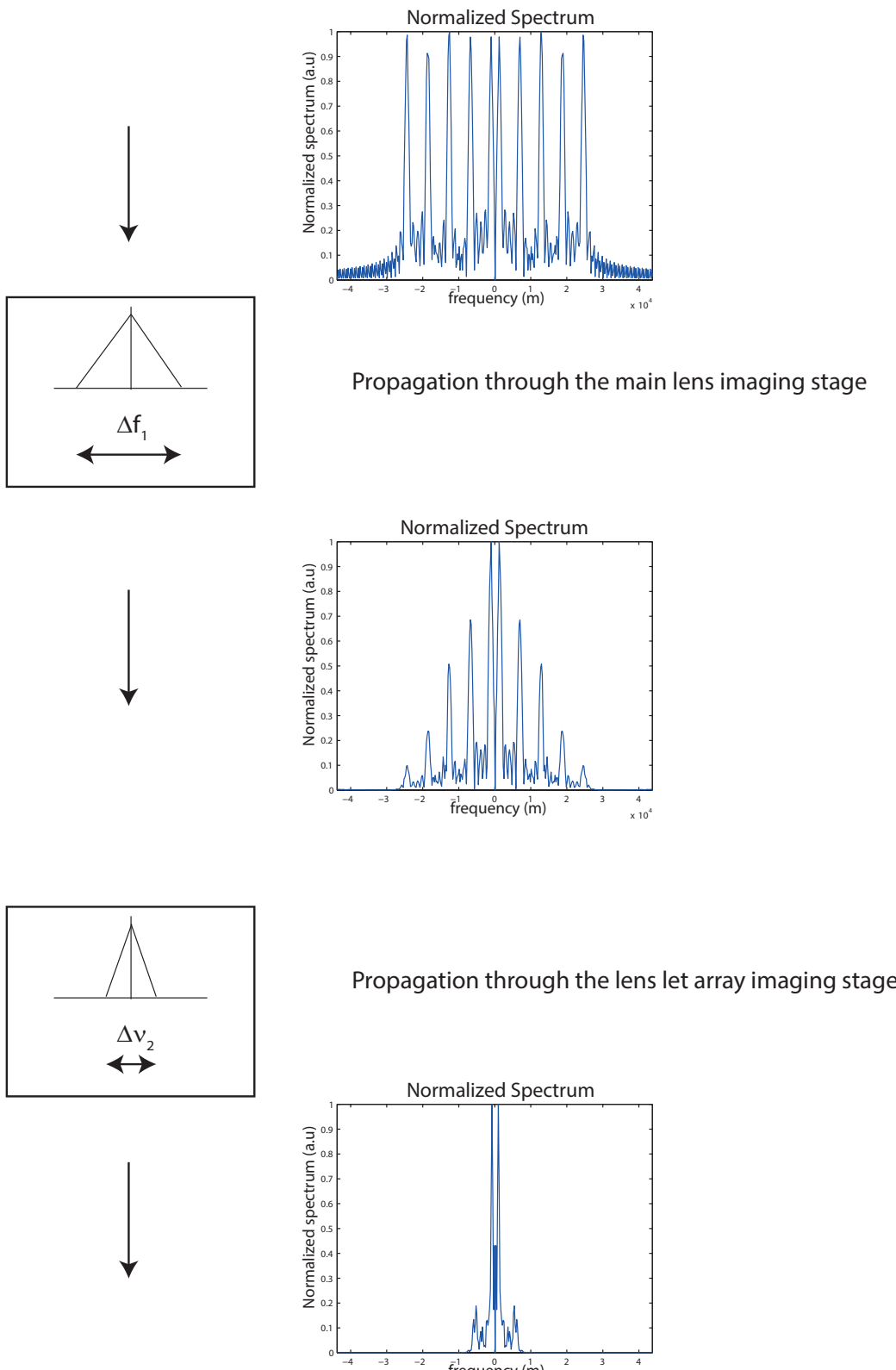


Figure 1.23: Evolution of the spectrum of the optical field as it propagates through the imaging system. First step the field is propagated through the main lens and its frequency content is modulated by its MTF whose bandwidth is $\Delta\nu_1$. Then modulated field passes through the lens let array stage and because of the magnification that is less than zero its bandwidth is reduced further to $\Delta\nu_2$. Since $\nu_1 < \nu_2$ the imaging system is modelled as a linear low pass filter with a bandwidth $\Delta\nu_1$ defined by the magnification of

It is interesting to see also that in the rendered image presents some artefacts which are responsible for some extra frequencies present in the spectrum of the output rendered image. The cut off frequency of the imaging system with a magnification equal to 0.5, is $10^4/m$, therefore only the first two frequencies will be transmitted to the rendered image, as shown in figure 1.22. If the magnification drops to $m = 0.3$ the bandwidth of the system gets narrower, and fewer frequencies are transmitted in the rendered image. Figure 1.24 shows the raw image, the main lens image and rendered images of the sinusoidal grating shown in figure 1.20

1.6. FREQUENCY ANALYSIS OF A FOCUSED PLENOPTIC SYSTEM 37

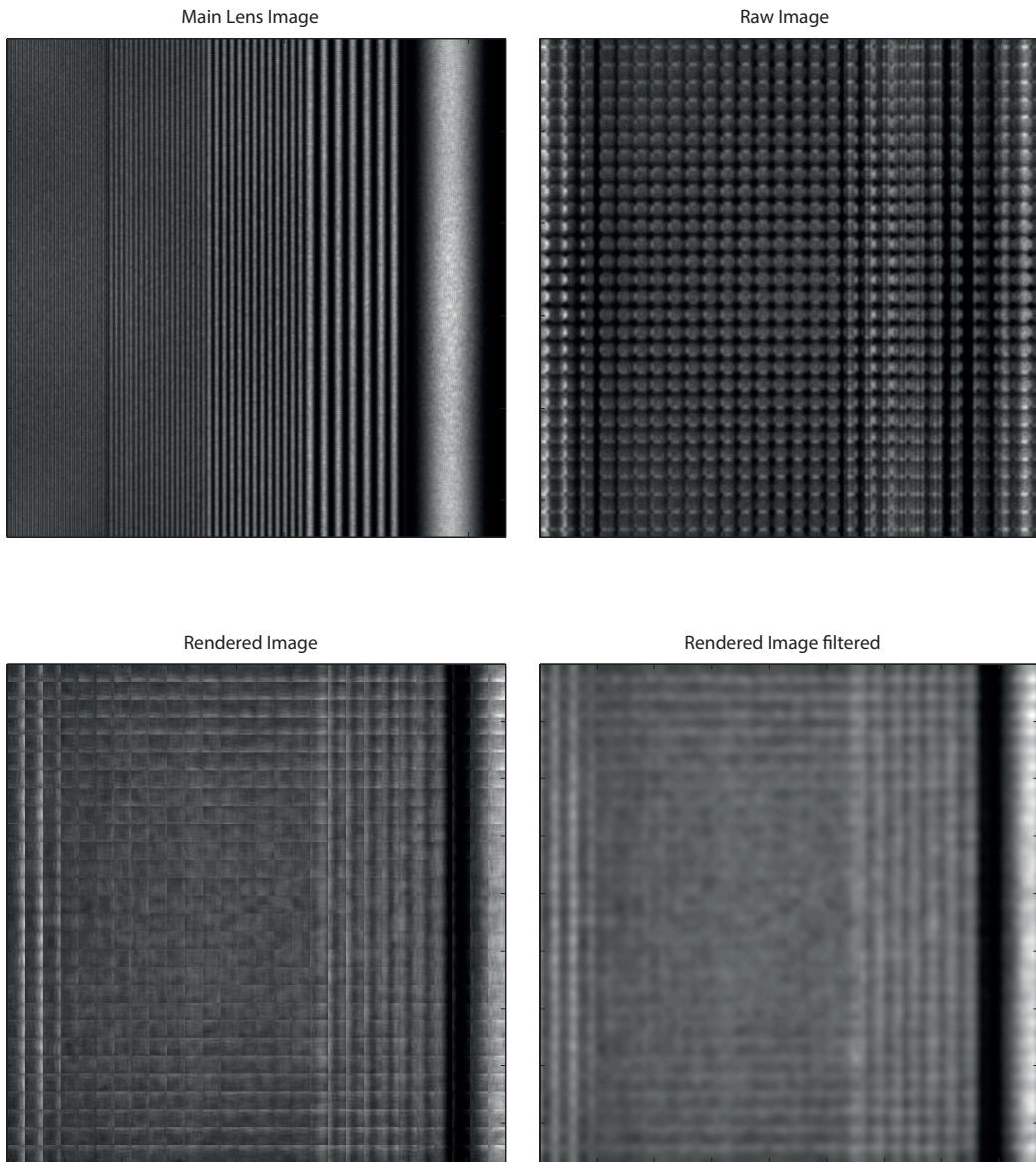


Figure 1.24: Top: on the left it is shown the raw sensor image, on the right the main lens image. Bottom: On the left there is the rendered image, on the right the same image has been low pass filtered to remove some of the rendering artefacts. Magnification was 0.3.

As for the previous case 1.25 shows a comparison of the intensity profile of the main lens image with the rendered image one and of their respective power spectra:

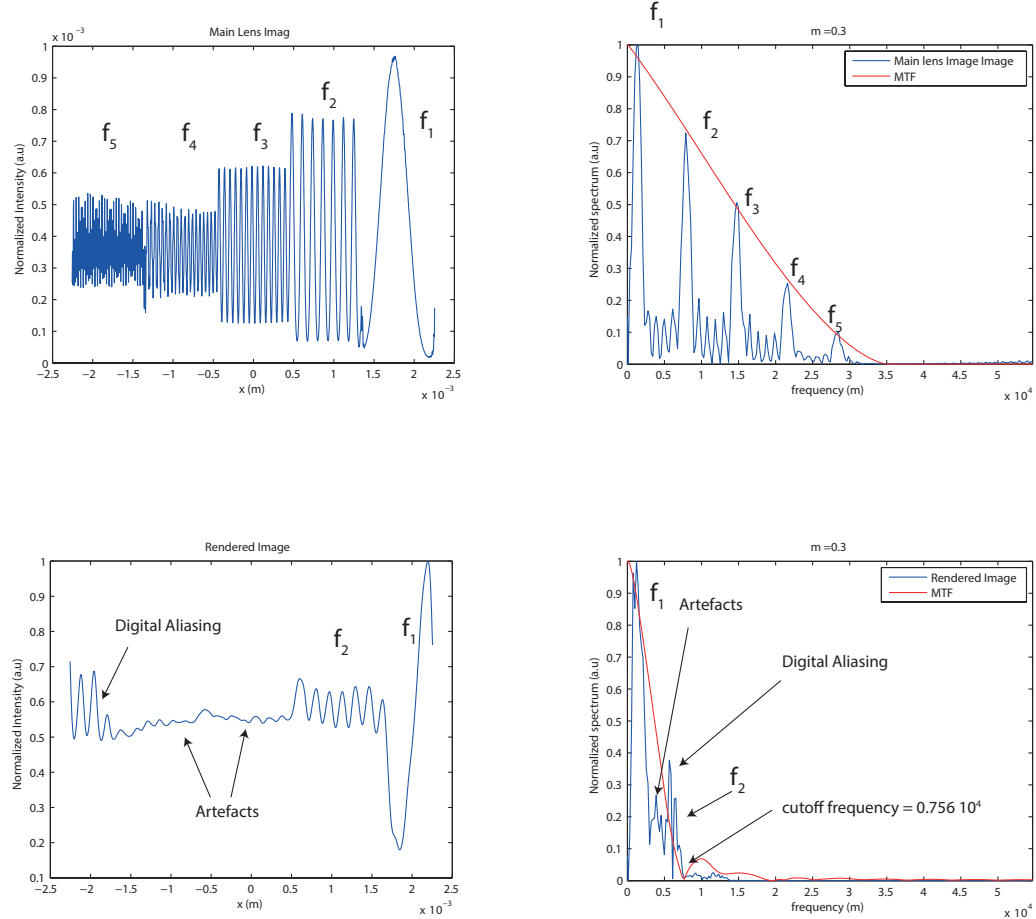


Figure 1.25: On the left: intensity profiles of the main lens image, top and of the rendered image, bottom. On the right: spatial frequency modulation done by MTF. The cut-off frequency of the system is $0.756 \times 10^4 \text{ m}^{-1}$

From figure 1.25 can be seen that the frequency f_2 gets attenuated more respect the previous case because it is closer to the cut-off frequency of the system. The spectrum of the rendered image allows to discriminate between frequencies due to artefacts and digital aliasing in the rendering process. Their frequency is smaller than the one predicted by the modulation transfer function for that location in the rendered image. These frequencies are

indicated in figure 1.25 with an arrow as artefacts. Low frequencies components generated by digital aliasing in the main lens image, have been picked up by the micro array relay stage and transmitted to the rendered image as indicated in figure 1.25. This effects can be seen in detail in figure 1.26:

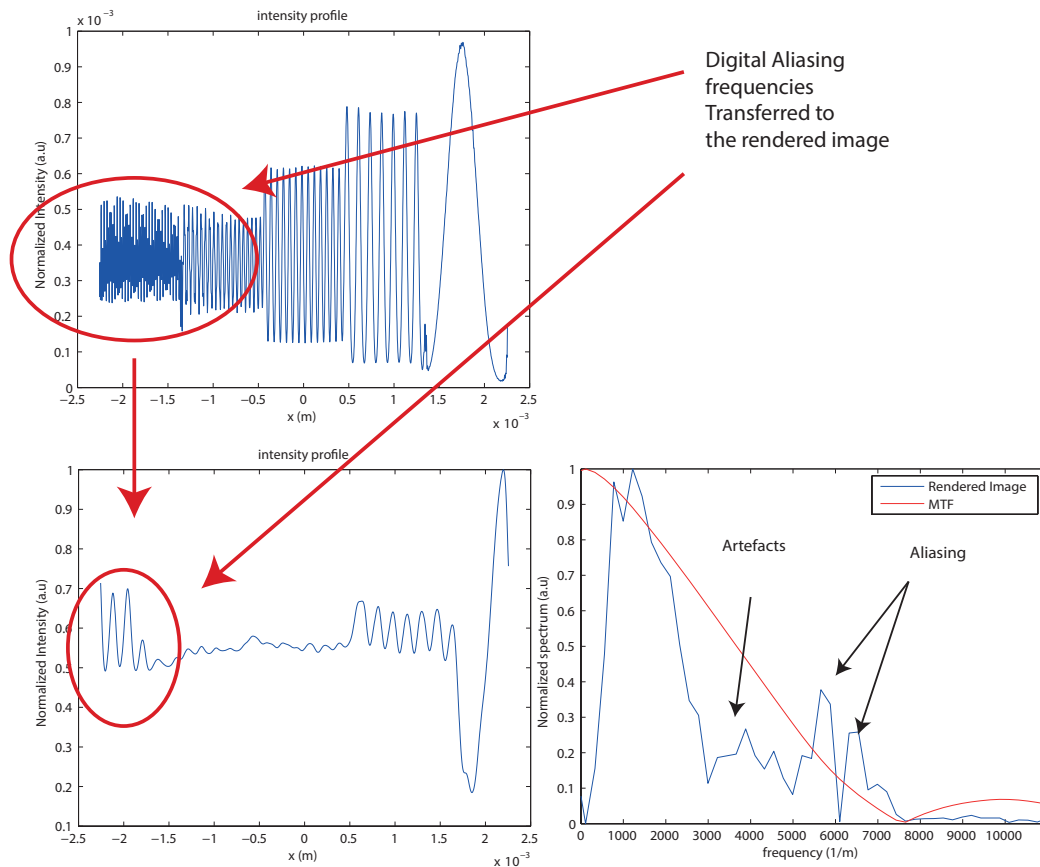


Figure 1.26: Aliased frequencies transmitted to the rendered image.

If the magnification is 0.25 the situation becomes the one in figure 1.27 and figure 1.28.

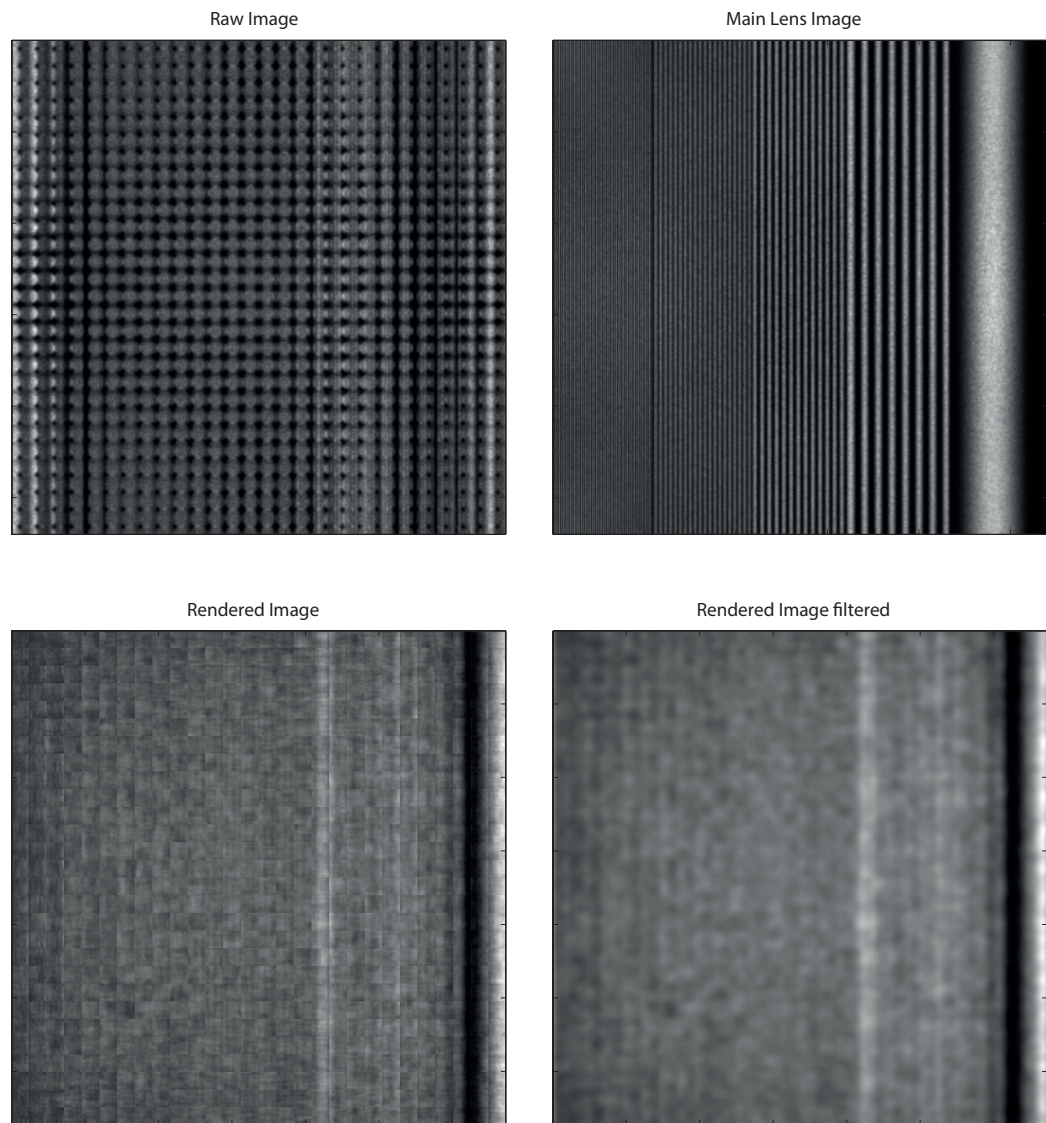


Figure 1.27: Top: raw sensor image, on the right the main lens image. Bottom: On the left there is the rendered image, on the right the same image has been low pass filtered to remove some of the rendering artefacts. Magnification was 0.3.

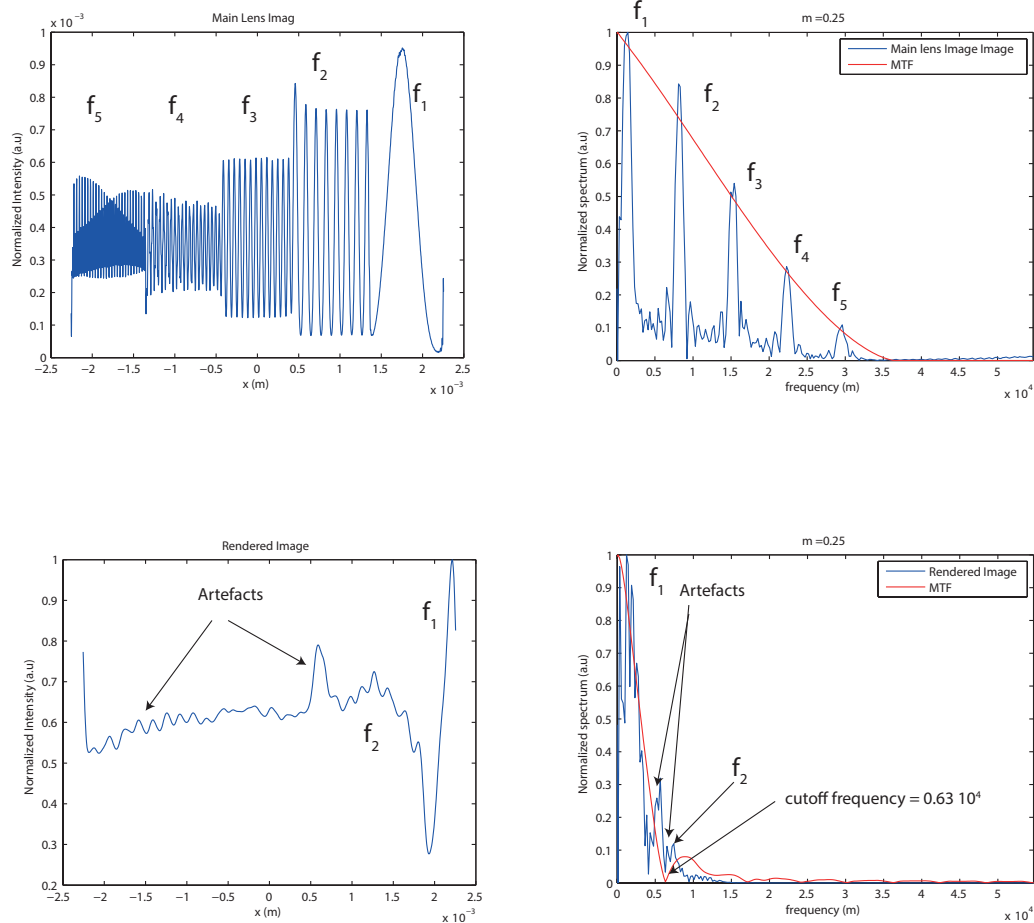


Figure 1.28: On the left: intensity profiles of the main lens image, top and of the rendered image, bottom. On the right there are the spatial frequencies modulated according to the MTF. The cut-off frequency of the system is $0.6 \times 10^4 1/m$

In the results shown in figure 1.28 there is a lower magnification and the digital aliasing frequencies are no longer transmitted to the rendered image. This is due to the fact that with a narrower bandwidth of the modulation transfer function these frequencies are filtered out of the signal. The same happens to the frequency f_2 of the object field, since the cut off frequency

for a magnification equal to 0.25 is lower than the signal frequency f_2 .

1.7 Conclusions

In this chapter has a frequency analysis of a focused plenoptic system has been done to investigate its behaviour at its diffraction limit. We analysed the optical performances of the plenoptic imaging system treating it as a linear system with a finite bandwidth that depends on the magnification of the lens let array. The distances a and b not only define the angular resolution of the system and the trade off with spatial resolution, but also allows to quantify the limits of the system in terms of optical resolution. This is a new contribution to the field, first presented in 2014 by Turola *et al.* [20]. Knowing how the optical frequencies are transmitted through the system allows to design its components in order to satisfy the requirements imposed by the practical application encountered. The optical resolution degradation with the increase of the angular resolution represents an intrinsic limitation to plenoptic 2.0 imaging system especially in applications regarding microscopy in which it is the diffraction that limits the resolution.

There are three ways to overcome this limitations: optically, computationally and hybrid one. The first approach consists in improving the basic optical elements of the system, that is choosing low f-number optical elements, larger array of micro lenses and sensors, or improving the optics before the micro array stage in order to deliver pre processed optical frequencies that will not be affected by the loss of resolution in the relay stage. It is also possible to act on the micro lens array, creating an array of lens lets with different focal length [27]. This approach could result in expensive devices, and it

is preferable to approach this issue computationally. Raw plenoptic data can be treated in post processing and can lead to a full sensor resolution rendering, and even a super resolution rendering as done by Georgiev *et al.* [31, 58, 63, 32, 64], by Favaro an Bishop [65, 66, 36, 29] and Shroff *et al.* [40, 30]. Another way to overcome the loss of resolution is to design a hybrid system composed by two branches, a plenoptic branch and and a conventional high resolution branch. This hybrid systems [67, 68], are based on the simultaneously acquisition of a plenoptic and a high resolution image, the latter being used as a base to interpolate the plenoptic data in order to fill the gaps in resolution.

In the next chapter the knowledge and the experience acquired designing and testing simulated plenoptic imaging system through simulation will be used to design a real optical setup, and the results obtained will be discussed.

Bibliography

- [1] Shree K Nayar. Computational cameras: Redefining the image. *Computer*, (8):30–38, 2006.
- [2] Ren Ng. *Digital light field photography*. PhD thesis, stanford university, 2006.
- [3] Todor Georgiev and Andrew Lumsdaine. Focused plenoptic camera and rendering. *Journal of Electronic Imaging*, 19(2):021106–021106, 2010.
- [4] Levoy Mark. Stanford light field microscope project, 2005.
- [5] Joseph Carroll, David B Kay, Drew Scoles, Alfredo Dubra, and Marco Lombardo. Adaptive optics retinal imaging-clinical opportunities and challenges. *Current eye research*, 38(7):709–721, 2013.
- [6] Gordon Wetzstein, Ivo Ihrke, Douglas Lanman, and Wolfgang Heidrich. Computational plenoptic imaging. In *Computer Graphics Forum*, volume 30, pages 2397–2426. Wiley Online Library, 2011.
- [7] Edward H Adelson and James R Bergen. *The plenoptic function and the elements of early vision*. Vision and Modeling Group, Media Laboratory, Massachusetts Institute of Technology, 1991.

- [8] Edward H Adelson and John Y. A. Wang. Single lens stereo with a plenoptic camera. *IEEE Transactions on Pattern Analysis & Machine Intelligence*, (2):99–106, 1992.
- [9] Plato and Francis Macdonald Cornford. *The republic of Plato*, volume 30. Oxford University Press New York, 1945.
- [10] Herbert E Ives. Parallax panoramagrams made with a large diameter lens. *J. Opt. Soc. Amer*, 20:332–342, 1930.
- [11] Frederic E Ives. Parallax stereogram and process of making same., April 14 1903. US Patent 725,567.
- [12] Lippmann Gabriel. La photographie intégrale. *Comptes-Rendus, Académie des Sciences*, 146:446–551, 1908.
- [13] Marc Levoy and Pat Hanrahan. Light field rendering. In *Proceedings of the 23rd annual conference on Computer graphics and interactive techniques*, pages 31–42. ACM, 1996.
- [14] Yuichi Taguchi, Amit Agrawal, Srikumar Ramalingam, and Ashok Veeraraghavan. Axial light field for curved mirrors: Reflect your perspective, widen your view. In *Computer Vision and Pattern Recognition (CVPR), 2010 IEEE Conference on*, pages 499–506. IEEE, 2010.
- [15] Steven J Gortler, Radek Grzeszczuk, Richard Szeliski, and Michael F Cohen. The lumigraph. In *Proceedings of the 23rd annual conference on Computer graphics and interactive techniques*, pages 43–54. ACM, 1996.

- [16] Bennett S Wilburn, Michal Smulski, Hsiao-Heng K Lee, and Mark A Horowitz. Light field video camera. In *Electronic Imaging 2002*, pages 29–36. International Society for Optics and Photonics, 2001.
- [17] Jason C Yang, Matthew Everett, Chris Buehler, and Leonard McMillan. A real-time distributed light field camera. *Rendering Techniques*, 2002:77–86, 2002.
- [18] Yoshikuni Nomura, Li Zhang, and Shree K Nayar. Scene collages and flexible camera arrays. In *Proceedings of the 18th Eurographics conference on Rendering Techniques*, pages 127–138. Eurographics Association, 2007.
- [19] Todor Georgiev, Ke Colin Zheng, Brian Curless, David Salesin, Shree Nayar, and Chintan Intwala. Spatio-angular resolution tradeoffs in integral photography. *Rendering Techniques*, 2006:263–272, 2006.
- [20] Massimo Turola and Steve Gruppetta. Wave optics simulations of a focused plenoptic system. In *Frontiers in Optics*, pages JTU3A–24. Optical Society of America, 2014.
- [21] Ren Ng, Marc Levoy, Mathieu Brédif, Gene Duval, Mark Horowitz, and Pat Hanrahan. Light field photography with a hand-held plenoptic camera. *Computer Science Technical Report CSTR*, 2(11), 2005.
- [22] Kensuke Ueda, Takafumi Koike, Keita Takahashi, and Takeshi Naemura. Adaptive integral photography imaging with variable-focus lens array. In *Electronic Imaging 2008*, pages 68031A–68031A. International Society for Optics and Photonics, 2008.

- [23] Ashok Veeraraghavan, Ramesh Raskar, Amit Agrawal, Ankit Mohan, and Jack Tumblin. Dappled photography: Mask enhanced cameras for heterodyned light fields and coded aperture refocusing. *ACM Trans. Graph.*, 26(3):69, 2007.
- [24] Douglas Lanman, Ramesh Raskar, Amit Agrawal, and Gabriel Taubin. Shield fields: modeling and capturing 3d occluders. *ACM Transactions on Graphics (TOG)*, 27(5):131, 2008.
- [25] Kshitij Marwah, Gordon Wetzstein, Yosuke Bando, and Ramesh Raskar. Compressive light field photography using overcomplete dictionaries and optimized projections. *ACM Transactions on Graphics (TOG)*, 32(4):46, 2013.
- [26] Yu Ji, Jinwei Ye, and Jingyi Yu. Depth reconstruction from the defocus effect of an xslit camera. In *Computational Optical Sensing and Imaging*, pages CM4E–3. Optical Society of America, 2015.
- [27] Todor Georgiev and Andrew Lumsdaine. The multifocus plenoptic camera. In *IS&T/SPIE Electronic Imaging*, pages 829908–829908. International Society for Optics and Photonics, 2012.
- [28] Todor Georgiev and Chintan Intwala. Light field camera design for integral view photography. *Adobe System, Inc*, 2006.
- [29] Tom E Bishop, Sara Zanetti, and Paolo Favaro. Light field superresolution. In *Computational Photography (ICCP), 2009 IEEE International Conference on*, pages 1–9. IEEE, 2009.

- [30] Sapna A Shroff and Kathrin Berkner. Image formation analysis and high resolution image reconstruction for plenoptic imaging systems. *Applied optics*, 52(10):D22–D31, 2013.
- [31] Todor Georgiev and Andrew Lumsdaine. Superresolution with plenoptic camera 2.0. *Adobe Systems Incorporated, Tech. Rep*, 2009.
- [32] Todor Georgiev. Plenoptic camera resolution. In *Computational Optical Sensing and Imaging*, pages JTh4A–2. Optical Society of America, 2015.
- [33] Changyin Zhou and Shree K Nayar. Computational cameras: Convergence of optics and processing. *Image Processing, IEEE Transactions on*, 20(12):3322–3340, 2011.
- [34] Andrew Lumsdaine and Todor Georgiev. Full resolution lightfield rendering. *Indiana University and Adobe Systems, Tech. Rep*, 2008.
- [35] Andrew Lumsdaine and Todor Georgiev. The focused plenoptic camera. In *Computational Photography (ICCP), 2009 IEEE International Conference on*, pages 1–8. IEEE, 2009.
- [36] Tom E Bishop and Paolo Favaro. Full-resolution depth map estimation from an aliased plenoptic light field. In *Computer Vision–ACCV 2010*, pages 186–200. Springer, 2011.
- [37] Todor G Georgiev and Andrew Lumsdaine. Resolution in plenoptic cameras. In *Computational Optical Sensing and Imaging*, page CTuB3. Optical Society of America, 2009.

- [38] Victor Guillemin and Shlomo Sternberg. *Symplectic techniques in physics*. Cambridge University Press, 1990.
- [39] Todor Georgiev, Andrew Lumsdaine, and Sergio Goma. Plenoptic principal planes. In *Imaging Systems and Applications*, page JTuD3. Optical Society of America, 2011.
- [40] Sapna Shroff and Kathrin Berkner. High resolution image reconstruction for plenoptic imaging systems using system response. In *Computational Optical Sensing and Imaging*, pages CM2B–2. Optical Society of America, 2012.
- [41] Gabriel C Birch, J Scott Tyo, and Jim Schwiegerling. Depth measurements through controlled aberrations of projected patterns. *Optics express*, 20(6):6561–6574, 2012.
- [42] Joyce E Farrell, Peter B Catrysse, and Brian A Wandell. Digital camera simulation. *Applied Optics*, 51(4):A80–A90, 2012.
- [43] Brian S Thurow and Timothy Fahringer. Recent development of volumetric piv with a plenoptic camera. In *PIV13; 10th International Symposium on Particle Image Velocimetry, Delft, The Netherlands, July 1-3, 2013*. Delft University of Technology, Faculty of Mechanical, Maritime and Materials Engineering, and Faculty of Aerospace Engineering, 2013.
- [44] Kyle Lynch. *Development of a 3-D fluid velocimetry technique based on light field imaging*. PhD thesis, Auburn University, 2011.

- [45] Kyle Lynch, Tim Fahringer, and Brian Thurow. Three-dimensional particle image velocimetry using a plenoptic camera. In *AIAA Aerospace Sciences Meeting*, 2012.
- [46] Arnold Sommerfeld. Optics lectures on theoretical physics, vol. iv. *Optics Lectures on Theoretical Physics, Vol. IV by Arnold Sommerfeld* New York, NY: Academic Press INC, 1954, 1, 1954.
- [47] Joseph W Goodman. *Introduction to Fourier optics*. Roberts and Company Publishers, 2005.
- [48] Maciej Sypek. Light propagation in the fresnel region. new numerical approach. *Optics communications*, 116(1):43–48, 1995.
- [49] Rafael C Gonzalez, Richard Eugene Woods, and Steven L Eddins. *Digital image processing using MATLAB*. Pearson Education India, 2004.
- [50] Kyoji Matsushima and Tomoyoshi Shimobaba. Band-limited angular spectrum method for numerical simulation of free-space propagation in far and near fields. *Optics express*, 17(22):19662–19673, 2009.
- [51] Maciej Sypek. Reply to the comment on “light propagation in the fresnel region–new numerical approach”. *Optics Communications*, 282(6):1074–1077, 2009.
- [52] Frank L Pedrotti and Leno S Pedrotti. Introduction to optics 2nd edition. *Introduction to Optics 2nd Edition by Frank L. Pedrotti, SJ, Leno S. Pedrotti* New Jersey: Prentice Hall, 1993, 1, 1993.

- [53] Joseph W Goodman and Randy L Haupt. *Statistical optics*. John Wiley & Sons, 2015.
- [54] Leonard Mandel and Emil Wolf. *Optical coherence and quantum optics*. Cambridge university press, 1995.
- [55] Max Born and Emil Wolf. *Principles of optics: electromagnetic theory of propagation, interference and diffraction of light*. Cambridge university press, 1999.
- [56] Emil Wolf. *Introduction to the Theory of Coherence and Polarization of Light*. Cambridge University Press, 2007.
- [57] Kensuke Ueda, Dongha Lee, Takafumi Koike, Keita Takahashi, and Takeshi Naemura. Multi-focal compound eye: liquid lens array for computational photography. In *ACM SIGGRAPH 2008 new tech demos*, page 28. ACM, 2008.
- [58] Todor G Georgiev and Andrew Lumsdaine. Super-resolution with the focused plenoptic camera, November 20 2012. US Patent 8,315,476.
- [59] Christian Perwass and Lennart Wietzke. Single lens 3d-camera with extended depth-of-field. In *Proc. SPIE*, volume 8291, page 829108, 2012.
- [60] Michael Hansen and Eric Holk. Depth map estimation for plenoptic images. 2011.
- [61] Ole Johannsen, Christian Heinze, Bastian Goldluecke, and Christian Perwass. On the calibration of focused plenoptic cameras. In *Time-of-*

- Flight and Depth Imaging. Sensors, Algorithms, and Applications*, pages 302–317. Springer, 2013.
- [62] Hans Peter Herzig. *Micro-optics: elements, systems and applications*. CRC Press, 1997.
- [63] Todor Georgiev, Georgi Chunev, and Andrew Lumsdaine. Superresolution with the focused plenoptic camera. In *IS&T/SPIE Electronic Imaging*, pages 78730X–78730X. International Society for Optics and Photonics, 2011.
- [64] Todor G Georgiev, Andrew Lumsdaine, and Sergio Goma. High dynamic range image capture with plenoptic 2.0 camera. In *Signal recovery and synthesis*, page SWA7P. Optical Society of America, 2009.
- [65] Paolo Favaro. A split-sensor light field camera for extended depth of field and superresolution. In *SPIE Photonics Europe*, pages 843602–843602. International Society for Optics and Photonics, 2012.
- [66] Tom E Bishop and Paolo Favaro. The light field camera: Extended depth of field, aliasing, and superresolution. *Pattern Analysis and Machine Intelligence, IEEE Transactions on*, 34(5):972–986, 2012.
- [67] Chien-Hung Lu, Stefan Muenzel, and Jason Fleischer. High-resolution light-field microscopy. In *Computational Optical Sensing and Imaging*, pages CTh3B–2. Optical Society of America, 2013.
- [68] Vivek Boominathan, Kaushik Mitra, and Ashok Veeraraghavan. Improving resolution and depth-of-field of light field cameras using a hybrid

- imaging system. In *Computational Photography (ICCP), 2014 IEEE International Conference on*, pages 1–10. IEEE, 2014.
- [69] Photonics for Innovations Quioptiq. *The Linos Catalog*. 2015.
- [70] August Köhler. A new system of illumination for photomicrographic purposes. *Z. Wiss. Mikroskopie*, 10:433–440, 1893.
- [71] August Kohler and Walter Bauersfeld. Device for light-field and dark-field illumination of microscopic objects, January 16 1934. US Patent 1,943,510.
- [72] Kurt Bernardo Wolf. *Geometric optics on phase space*. Springer Science & Business Media, 2004.